

Isotope Shifts in Beryllium-, Boron-, Carbon-, and Nitrogen-like Ions from Relativistic Configuration Interaction Calculations

C. Nazé^{a,*}, S. Verdebout^a, P. Rynkun^b, G. Gaigalas^b, M. Godefroid^a, P. Jönsson^c

^a*Service de Chimie Quantique et Photophysique, CP160/09,*

Université Libre de Bruxelles, Avenue F.D. Roosevelt 50, B 1050 Brussels, Belgium

^b*Vilnius University, Institute of Theoretical Physics and Astronomy, LT-01108 Vilnius, Lithuania*

^c*Group for Materials Science and Applied Mathematics, Malmö University, 205-06 Malmö, Sweden*

Abstract

Energy levels, normal and specific mass shift parameters as well as electronic densities at the nucleus are reported for numerous states along the beryllium, boron, carbon, and nitrogen isoelectronic sequences. Combined with nuclear data, these electronic parameters can be used to determine values of level and transition isotope shifts. The calculation of the electronic parameters is done using first-order perturbation theory with relativistic configuration interaction wave functions that account for valence, core-valence and core-core correlation effects as zero-order functions. Results are compared with experimental and other theoretical values, when available.

arXiv:1406.1720v1 [physics.atom-ph] 6 Jun 2014

*Corresponding author.

Email address: mrgodef@ulb.ac.be (M. Godefroid)

Contents

1. Introduction	3
2. Isotope shift theory	3
2.1. Mass shift	4
2.2. Field shift	5
2.3. Total line frequency shift	6
3. Computational procedure	6
3.1. Multiconfiguration Dirac-Hartree-Fock	6
3.2. Computation of isotope shift parameters	7
4. Generation of configurations expansions	7
4.1. Boron-, carbon-, and nitrogen-like systems	7
4.2. Beryllium-like systems	8
5. Results and data evaluation	9
5.1. Beryllium-like ions	9
5.2. Boron-like ions	10
5.3. Carbon-like ions	11
5.4. Nitrogen-like ions	12
6. Outlook and conclusion	12
References	13
Explanation of Tables	16
Tables	
1. Total energies (in E_h), excitation energies (in cm^{-1}), normal and specific mass shift \tilde{K} parameters (in GHz u), \tilde{F} field shift factors (in GHz/fm^2) for levels in the beryllium isoelectronic sequence ($5 \leq Z \leq 74$). For each of the many-electron wave functions, the leading components are given in the LSJ coupling scheme. The number in square brackets is the power of 10. See page 16 for Explanation of Tables.	19
2. Total energies (in E_h), excitation energies (in cm^{-1}), normal and specific mass shift \tilde{K} parameters (in GHz u), \tilde{F} field shift factors (in GHz/fm^2) for levels in the boron isoelectronic sequence ($8 \leq Z \leq 30$ and $Z = 36, 42$). For each of the many-electron wave functions, the leading components are given in the LSJ coupling scheme. The number in square brackets is the power of 10. See page 17 for Explanation of Tables.	33
3. Total energies (in E_h), excitation energies (in cm^{-1}), normal and specific mass shift \tilde{K} parameters (in GHz u), \tilde{F} field shift factors (in GHz/fm^2) for levels in the carbon isoelectronic sequence ($7 \leq Z \leq 28$). For each of the many-electron wave functions, the leading components are given in the LSJ coupling scheme. The number in square brackets is the power of 10. See page 17 for Explanation of Tables.	40
4. Total energies (in E_h), excitation energies (in cm^{-1}), normal and specific mass shift \tilde{K} parameters (in GHz u), \tilde{F} field shift factors (in GHz/fm^2) for levels in the nitrogen isoelectronic sequence ($7 \leq Z \leq 36$ and $Z = 42, 74$). For each of the many-electron wave functions, the leading components are given in the LSJ coupling scheme. The number in square brackets is the power of 10. See page 18 for Explanation of Tables.	49

1. Introduction

High resolution solar and stellar spectra reveal isotope shifts (IS) and hyperfine structures of many spectral lines. These small structures are not always completely resolved and instead they shift and broaden the atomic lines. To correctly interpret the spectra it is often necessary to include isotope shifts and hyperfine structures in a theoretical modeling of the line profiles [1, 2]. Hyperfine and isotope data are also needed for generating synthetic spectra to study isotope anomalies in astronomical objects [3] and for understanding nucleosynthesis mechanisms [4, 5]. In the last decade, several studies have shown that the typical isotope shifts may be of the same order of magnitude as the effects of the possible temporal and spatial variation of the fine-structure constant. In this framework, Kozlov *et al.* [6] proposed a method to exclude systematic effects caused by changes in the isotope abundances during the evolution of the universe, but there is a need to develop methods that can accurately estimate isotope shifts [7]. Isotope shifts of spectral lines are also used in nuclear physics to estimate the root-mean-square nuclear charge radii and mean-square radii changes $\delta\langle r^2 \rangle^{A,A'}$ for which the electronic factors play a crucial role (see for example [8–12]).

Relativistic effects on the electronic structure are expected to increase with the nuclear charge. Shabaev [13, 14] and, in an independent way, Palmer [15], derived relativistic corrections to the mass shift. Since then several papers have shown the importance of relativistic effects on isotope shifts [16–20]. The development of experimental techniques allowing the accurate measurement of line IS enhances the need for accurate calculations of the relevant electronic parameters that account for both electron correlation and relativistic effects, especially for medium and heavy open-shell atoms [21, 22]. Amongst these techniques, the storage ring measurement of isotope shifts in the spectrum of resonant electron-ion recombination of heavy few-electron ions gives access to nuclear charge radii changes involving heavy stable and unstable nuclides, as demonstrated for three-electron Nd⁵⁷⁺ isotopes produced at GSIs storage ring ESR [8]. Dielectronic recombination (DR) measurements have also been performed at the heavy-ion storage ring TSR in Heidelberg for Be-, B- and C-like ions relevant to astrophysics and plasma physics [23, 24], although no IS in the DR spectra have been reported so far. DR experiments are also envisaged at ISOLDE [25] where the availability of radioisotopes together with the TSR electron collision facilities will open up new opportunities.

GRASP2K [26] is a fully relativistic code based on the multiconfiguration Dirac-Hartree-Fock (MCDHF) method. Its latest release [27] includes a module, RIS3 [28], that evaluates the isotope shift parameters including the relativistic corrections to the recoil operator as derived by Shabaev [13, 14]. The purpose of the present work is to complement the available atomic data sets along the beryllium, boron, carbon and nitrogen isoelectronic sequences with accurate IS electronic parameters that can be used for modeling high resolution stellar spectra, and for interpreting future measurements of isotope effects that would require the knowledge of the electronic factors to access the nuclear charge radii.

2. Isotope shift theory

An atomic spectral line is characteristic of the element producing the spectrum. The frequency of a spectral line k connecting levels $\ell \leftrightarrow u$, with $E_u > E_\ell$, is given by

$$\nu_k = \frac{E_u - E_\ell}{h}, \quad (1)$$

and differs from one isotope to another. The line frequency isotope shift between isotopes A and A' (with $A > A'$) is

$$\delta\nu_k^{A,A'} \equiv \nu_k^A - \nu_k^{A'} = \frac{\delta E_u^{A,A'} - \delta E_\ell^{A,A'}}{h}, \quad (2)$$

with

$$\delta E_i^{A,A'} = E_i^A - E_i^{A'} \quad (i = \ell, u). \quad (3)$$

The isotope shift is made up of two effects: the mass shift (MS) and the field shift (FS). Generally, the FS dominates for heavy atoms whereas the MS plays a prominent role for light atoms. In the present work, both effects are expressed as expectation values of operators that are calculated through first-order perturbation theory [29] using approximate solutions of the fully relativistic Dirac-Hartree-Fock(-Breit) Hamiltonian as zero-order wave functions.

2.1. Mass shift

The finite mass of the nucleus gives rise to a recoil effect, called the mass shift. The nuclear recoil corrections within the $(\alpha Z)^4 m^2/M$ approximation are obtained by evaluating the expectation values of the operator [16, 30]

$$H_{\text{MS}} = \frac{1}{2M} \sum_{i,j}^N \left(\mathbf{p}_i \cdot \mathbf{p}_j - \frac{\alpha Z}{r_i} \boldsymbol{\alpha}_i \cdot \mathbf{p}_j - \frac{\alpha Z}{r_i} \frac{(\boldsymbol{\alpha}_i \cdot \mathbf{r}_i) \mathbf{r}_i}{r_i^2} \cdot \mathbf{p}_j \right). \quad (4)$$

Separating the one-body ($i = j$) and two-body terms ($i \neq j$) into the normal mass shift (NMS) and specific mass shift (SMS) respectively, the expression (4) splits in

$$H_{\text{MS}} = H_{\text{NMS}} + H_{\text{SMS}}. \quad (5)$$

For a given atomic state i , the (mass-independent) normal mass shift K_{NMS} and specific mass shift K_{SMS} parameters are defined by the following expressions

$$K_{i,\text{NMS}} \equiv M \langle \Psi_i | H_{\text{NMS}} | \Psi_i \rangle, \quad (6)$$

$$K_{i,\text{SMS}} \equiv M \langle \Psi_i | H_{\text{SMS}} | \Psi_i \rangle. \quad (7)$$

These mean values can be expressed as

$$K_{\text{NMS}} = K_{\text{NMS}}^1 + K_{\text{NMS}}^2 + K_{\text{NMS}}^3$$

and

$$K_{\text{SMS}} = K_{\text{SMS}}^1 + K_{\text{SMS}}^2 + K_{\text{SMS}}^3,$$

where each contribution refers to one of the three terms appearing in (4). More complete developments, as well as the derivation of the tensorial form of (4), are detailed in the work of Gaidamaukas *et al.* [31].

The corresponding level mass shift between two isotopes A and A' with masses M and M' , respectively, can be written

$$\delta E_{i,\text{MS}}^{A,A'} = \left(\frac{1}{M} - \frac{1}{M'} \right) (K_{i,\text{NMS}} + K_{i,\text{SMS}}), \quad \text{with } A > A'. \quad (8)$$

In atomic units, the nuclear masses M and M' that are usually given in units of the unified atomic mass (u), must be converted to atomic units of mass (m_e) to be consistent with K factors expressed in [$m_e E_h$] units. For discussing the

transition isotope shift (2), one needs to consider the variation of the mass parameter from one level to another. The corresponding line frequency isotope mass shift is written as the sum of the NMS and SMS contributions:

$$\delta\nu_{k,\text{MS}}^{A,A'} = \delta\nu_{k,\text{NMS}}^{A,A'} + \delta\nu_{k,\text{SMS}}^{A,A'} , \quad (9)$$

with

$$\delta\nu_{k,\text{MS}}^{A,A'} = \left(\frac{M' - M}{MM'} \right) \frac{\Delta K_{\text{MS}}}{h} = \left(\frac{M' - M}{MM'} \right) \Delta \tilde{K}_{\text{MS}} , \quad (10)$$

where $\Delta K_{\text{MS}} = (K_{u,\text{MS}} - K_{\ell,\text{MS}})$ is the difference of the $K_{\text{MS}} (= K_{\text{NMS}} + K_{\text{SMS}})$ parameters of the upper (u) and lower (ℓ) levels involved in the transition k . For $\Delta \tilde{K}_{\text{MS}}$, the unit (GHz u) is often used in the literature. As far the conversion factor is concerned, we use $\Delta K_{\text{MS}}[m_e E_h] = 3609.4824 \Delta \tilde{K}_{\text{MS}}[\text{GHz u}]$.

2.2. Field shift

The energy shift arising from the difference in nuclear charge distributions between two isotopes A and A' for a given atomic state i is called the level field shift. Neglecting higher order isotopic variation of the nuclear charge distribution, the level field shift can be written [29, 32]

$$\delta E_{i,\text{FS}}^{A,A'} = (h\tilde{\mathcal{F}}_i) \delta \langle r^2 \rangle^{A,A'} , \quad (11)$$

where

$$\delta \langle r^2 \rangle^{A,A'} = \langle r^2 \rangle^A - \langle r^2 \rangle^{A'} \quad (12)$$

is the difference of the nuclear root-mean-square (rms) charge radii involved. The level field shift electronic factor $\tilde{\mathcal{F}}_i$ is given (in units of frequency divided by a length squared) by

$$\tilde{\mathcal{F}}_i = \frac{2\pi}{3h} Z \left(\frac{e^2}{4\pi\epsilon_0} \right) |\Psi(0)|_i^2 , \quad (13)$$

where $|\Psi(0)|^2$ is the total probability density at the origin that can be estimated by taking the ($\mathbf{r} \rightarrow \mathbf{0}$) limit of the electron density [28] (see section 3.1)

$$|\Psi(0)|_i^2 = \lim_{\mathbf{r} \rightarrow \mathbf{0}} \rho_i^e(\mathbf{r}) = \frac{1}{4\pi} \lim_{r \rightarrow 0} \rho_i^e(r) . \quad (14)$$

Using (11) for levels $i = (\ell, u)$ involved in transition k , the frequency field shift of the spectral line k can be written as [29, 32, 33]

$$\delta\nu_{k,\text{FS}}^{A,A'} = \frac{\delta E_{u,\text{FS}}^{A,A'} - \delta E_{\ell,\text{FS}}^{A,A'}}{h} = F_k \delta \langle r^2 \rangle^{A,A'} . \quad (15)$$

F_k is the line electronic factor (in units of frequency divided by a length squared)

$$F_k = \frac{2\pi}{3h} Z \left(\frac{e^2}{4\pi\epsilon_0} \right) \Delta |\Psi(0)|_k^2 , \quad (16)$$

proportional to the change of the total probability density at the origin associated with the electronic transition between levels ℓ and u . In this approximation, the first-order level- and frequency-field shifts (11) and (15) become

$$\delta E_{i,\text{FS}}^{A,A'} = (h\tilde{\mathcal{F}}_i) \delta \langle r^2 \rangle^{A,A'} = \frac{2\pi}{3} Z \left(\frac{e^2}{4\pi\epsilon_0} \right) |\Psi(0)|_i^2 \delta \langle r^2 \rangle^{A,A'} , \quad (17)$$

and

$$\delta\nu_{k,\text{FS}}^{A,A'} = F_k \delta \langle r^2 \rangle^{A,A'} = \frac{Z}{3h} \left(\frac{e^2}{4\pi\epsilon_0} \right) \Delta |\Psi(0)|_k^2 \delta \langle r^2 \rangle^{A,A'} , \quad (18)$$

respectively. The wavenumber ($\sigma = E/hc$) field shift

$$\delta\sigma_{k,\text{FS}}^{A,A'} = \frac{Z}{3\hbar c} \left(\frac{e^2}{4\pi\epsilon_0} \right) \Delta|\Psi(0)|_k^2 \delta\langle r^2 \rangle^{A,A'}, \quad (19)$$

is also often used by experimentalists.

2.3. Total line frequency shift

One can estimate the total line frequency shift by merely adding the mass shift (10) and field shift (15) contributions¹

$$\begin{aligned} \delta\nu_k^{A,A'} &= \underbrace{\delta\nu_{k,\text{NMS}}^{A,A'} + \delta\nu_{k,\text{SMS}}^{A,A'}}_{\delta\nu_{k,\text{MS}}^{A,A'}} + \delta\nu_{k,\text{FS}}^{A,A'} \\ &= \left(\frac{M' - M}{MM'} \right) \Delta\tilde{K}_{\text{MS}} + F_k \delta\langle r^2 \rangle^{A,A'}. \end{aligned} \quad (20)$$

3. Computational procedure

3.1. Multiconfiguration Dirac-Hartree-Fock

The multiconfiguration Dirac-Hartree-Fock (MCDHF) method [34], as implemented in the program package GRASP2K [26, 27], is used to obtain approximate wave functions describing the atomic levels. An atomic state function (ASF) is represented by a linear combination of configuration state functions (CSFs) with same parity P , total angular momentum J , and its component along z -direction, M_J ,

$$\Psi(\gamma P J M_J) = \sum_{j=1}^{NCSF} c_j \Phi(\gamma_j P J M_J), \quad (21)$$

where $\{c_j\}$ are the mixing coefficients and $\{\gamma_j\}$ the sets of configuration and intermediate shell-coupling quantum numbers needed to unambiguously specify the CSFs. The latter are built on single-electron Dirac spinors. The mixing coefficients and the single-electron orbitals (radial large and small components) are obtained by iteratively solving the relativistic self-consistent field (RSCF) equations and the secular equation associated with the configuration interaction matrix. A more limited version is the relativistic configuration interaction (RCI) approach using a fixed pre-optimized set of orbitals and allowing only the mixing coefficients to be varied. In the RCI computation, the Breit interaction and leading QED effects (the vacuum polarization and self-energy) can be taken into account perturbatively as well. It should be emphasized that the use of a point-like nucleus gives unreliable electron densities at the nucleus in the relativistic scheme. A finite nuclear charge distribution model should be used instead to ensure the first-order perturbation to be valid for the field shift [29]. In the present work, the two-parameters (c, a) Fermi nuclear model

$$\rho(r) = \frac{\rho_0}{1 + e^{(r-c)/a}} \quad (22)$$

is adopted to generate the nuclear potential felt by the electrons. Here ρ_0 is a normalization coefficient, c is the half-density radius and $a = t/(4 \ln 3)$ is related to the surface thickness t of the charge distribution. In practice, the value $t = 2.30$ fm is used and c is computed according to the formulae given in [35]. Since the ASFs are relatively insensitive

¹The line frequency shift (20) is often written as $\delta\nu_k^{A,A'} = M_k \frac{A'-A}{AA'} + F_k \delta\langle r^2 \rangle^{A,A'}$

to the details of the nuclear model, the nuclear parameters from any stable isotope of the considered chemical element ${}_Z X$ can be safely chosen for performing the MCDHF and RCI calculations of the electronic wave functions. As discussed by Blundell *et al.* [29], and as confirmed by more recent studies (see for instance [36]), the error inherent to the use of a first-order perturbation picture that neglects changes in the electron wave functions arising from variations in the nuclear charge distribution, is estimated of the order of one part in 10^3 - 10^4 .

3.2. Computation of isotope shift parameters

The isotope shift parameters and the electron density at the nucleus are calculated in a first-order perturbation approach using the MCDHF or RCI atomic state functions as the zero-order wave functions. Rewriting the operators for the normal mass shift parameter K_{NMS} , the specific mass shifts parameter K_{SMS} as well as for the electron density in tensorial form [31], the calculation of these quantities reduces to a summation over matrix elements between CSFs. These matrix elements, in turn, are expressed as sums over radial integrals weighted by angular factors. All isotope shift electronic parameters were calculated using the isotope shift module RIS3 [28] interfaced with the GRASP2K package [27]. Angular factors were saved on disk and re-used for all ions in an isoelectronic sequence to reduce the execution time.

4. Generation of configurations expansions

MCDHF and RCI calculations can be performed for single levels, but also for portions of a spectrum. In this work calculations were carried out by parity and configuration, that is, wave functions for all states belonging to a specific configuration were determined simultaneously in an EOL calculation [37]. Using the latter scheme, a balanced description of a number of fine-structure states belonging to one or more configurations can be obtained in a single calculation. The expansions for the ASFs were obtained using the active set method [38]. Here CSFs of a specified parity and J -symmetry are generated by excitations from a number of reference configurations to a set of relativistic orbitals. By applying restrictions on the allowed excitations, different electron correlation effects can be targeted. To monitor the convergence of the calculated energies and the physical quantities of interest, the active sets are increased in a systematic way by progressively adding layers of correlation orbitals.

4.1. Boron-, carbon-, and nitrogen-like systems

The starting point was a number of MCDHF calculations where the CSF expansions for the states belonging to a configuration were obtained by single and double (SD) excitations from a multireference (MR) consisting of the set of configurations that can be formed by the same principal quantum numbers as the studied configuration, to an increasing active set of orbitals. The MCDHF calculations were followed by RCI calculations including the Breit interaction and leading QED. The CSF expansions for the RCI calculations were obtained by SD-excitations from a larger MR, including the most important configurations outside the complex, to the largest active set of orbitals. The correlation models used for the boron-, carbon-, and nitrogen-like ions are summarized in Table A. The reference configuration is shown on the left. Columns two and three display the MR for, respectively, the MCDHF and RCI expansions. The largest active set is shown in column four, where the number of orbitals for each l -angular symmetry is specified. The last column gives the number of CSFs for the RCI calculations. The described computational strategy has previously been used by Rynkun *et al.* [39–41] to compute energies and transition rates, and more details can be found in these papers.

Table A

Generated CSF expansions for the MCDHF and RCI calculations for the boron-, carbon-, and nitrogen-like ions.

Configuration	MR for MCDHF	MR for RCI	Active set	NCSF in RCI
boron-like				
$1s^2 2s^2 2p$	$1s^2\{2s^2 2p, 2p^3\}$	$1s^2\{2s^2 2p, 2p^3, 2s 2p 3d, 2p 3d^2\}$	$\{9s 8p 7d 6f 5g 3h 1i\}$	$200 \cdot 10^3$
$1s^2 2p^3$	$1s^2\{2s^2 2p, 2p^3\}$	$1s^2\{2s^2 2p, 2p^3, 2s 2p 3d, 2p 3d^2\}$	$\{9s 8p 7d 6f 5g 3h 1i\}$	$360 \cdot 10^3$
$1s^2 2s 2p^2$	$1s^2 2s 2p^2$	$1s^2\{2s 2p^2, 2p^2 3d, 2s^2 3d, 2s 3d^2\}$	$\{9s 8p 7d 6f 5g 3h 1i\}$	$300 \cdot 10^3$
carbon-like				
$1s^2 2s^2 2p^2$	$1s^2\{2s^2 2p^2, 2p^4\}$	$1s^2\{2s^2 2p^2, 2p^4, 2s 2p^2 3d, 2s^2 3d^2\}$	$\{8s 7p 6d 5f 4g 2h\}$	$340 \cdot 10^3$
$1s^2 2p^4$	$1s^2\{2s^2 2p^2, 2p^4\}$	$1s^2\{2s^2 2p^2, 2p^4, 2s 2p^2 3d, 2s^2 3d^2\}$	$\{8s 7p 6d 5f 4g 2h\}$	$340 \cdot 10^3$
$1s^2 2s 2p^3$	$1s^2 2s 2p^3$	$1s^2\{2s 2p^3, 2p^3 3d, 2s^2 2p 3d, 2s 2p 3d^2\}$	$\{8s 7p 6d 5f 4g 2h\}$	$1\,000 \cdot 10^3$
nitrogen-like				
$1s^2 2s^2 2p^3$	$1s^2\{2s^2 2p^3, 2p^5\}$	$1s^2\{2s^2 2p^3, 2p^5, 2s 2p^3 3d, 2s^2 2p 3d^2\}$	$\{8s 7p 6d 5f 4g 1h\}$	$698 \cdot 10^3$
$1s^2 2p^5$	$1s^2\{2s^2 2p^3, 2p^5\}$	$1s^2\{2s^2 2p^3, 2p^5, 2s 2p^3 3d, 2s^2 2p 3d^2\}$	$\{8s 7p 6d 5f 4g 1h\}$	$382 \cdot 10^3$
$1s^2 2s 2p^4$	$1s^2 2s 2p^4$	$1s^2\{2s 2p^4, 2p^4 3d, 2s^2 2p^2 3d, 2s 2p^2 3d^2\}$	$\{8s 7p 6d 5f 4g 1h\}$	$680 \cdot 10^3$

4.2. Beryllium-like systems

The beryllium-like systems are a little different. For each parity, the wave functions for all states belonging to the $1s^2 2s^2$ and $1s^2 2p^2$ even configurations, and to the $1s^2 2s 2p$ odd configuration, were determined simultaneously. For the MCDHF calculations, the CSF expansions were obtained by merging CSFs generated by SD-excitations from the reference configurations to an increasing active set with CSFs obtained by single, double, triple, and quadruple (SDTQ) excitations to a subset of the active set of orbitals. The largest active set consisted of orbitals with principal quantum numbers $n \leq 8$ and the subset was formed by orbitals with principal quantum numbers $n \leq 4$. The MCDHF calculations were followed by RCI calculations including the Breit interaction and leading QED. The expansions for the RCI calculations were obtained by merging CSFs generated by SDTQ-excitations from the reference configurations to the largest active set with the restriction that there in each CSF is at least two orbitals with $n \leq 3$ with CSFs generated by SDTQ-excitations from the reference configurations to the active set of orbitals with principal quantum numbers $n \leq 4$. The RCI expansions included about 296 000 relativistic CSFs.

5. Results and data evaluation

In the following subsections, the results of the calculations are presented for the four isoelectronic sequences, and compared with values from the available literature.

The identification of the levels is based on the LS composition obtained by transforming from jj - to LS -coupling schemes using the JJ2LSJ tool integrated in the new release of GRASP2K [27]. The two first CSFs with weight $|c_j|^2 \geq 0.1\%$ are also displayed in the level compositions. All the IS electronic parameters reported in the tables have been estimated using RIS3 and the correspondence with the LSJ levels has been done using the tool RIS3_LSJ [28].

5.1. Beryllium-like ions

Table 1 gives the total energies, the transition energies, the \tilde{K}_{NMS} and \tilde{K}_{SMS} parameters, and the electronic field shift factors \tilde{F} for levels in beryllium-like ions ($5 \leq Z \leq 74$) from RCI calculations described in the previous section. It must be stressed that the level $2p^2 \ ^1S_0$ of the B II ion required a special attention. For this excited state, the influence of the triple and quadruple excitations is strong and limiting the population as described in section 4.2 becomes inadequate. The results presented are those of an expansion based on SDTQ-excitations up to $n = 7i$.

Table 2 presents a comparison with theoretical and experimental results of Litzén *et al.* [42] for B II, for which multiconfiguration Hartree-Fock (MCHF) calculations were performed in a non-relativistic scheme with the program ATSP2K [43]. Expecting a small contribution of orbitals with high angular momenta, the latter were limited to $l \leq 3$. The $\delta\sigma_{\text{FS}}$ values evaluated from (19) and using the experimental nuclear rms charge radius of Angeli [44], are reported in the last column. No data are available in the literature, but these numbers illustrate how small the FS is for the B II ion. An analysis of the 1362 Å line profile observed in Hubble spectra of the interstellar medium indicated an IS of 13.7 ± 3.5 mÅ for the transition $2s^2 \ ^1S_0 - 2s2p \ ^1P_1^o$ [45] for the pair $^{11}\text{B}-^{10}\text{B}$; converting our value $\delta\sigma_{\text{MS}} = 0.711 \text{ cm}^{-1}$ gives $\delta\lambda = 13.20$ mÅ. As the values obtained by Litzén *et al.* are 13 mÅ and 13.27 mÅ for experiment and theory respectively, all values are within experimental error bars of the Hubble observation. Except for the transition $2s2p \ ^1P_1^o - 2p^2 \ ^1S_0$, values are in good agreement with both experiments and previous theoretical work. The source of the discrepancy has been investigated in details and is attributed to the incomplete correlation model adopted in [42].

Table 3 gives a comparison with the calculations of Korol and Kozlov [17], Jönsson *et al.* [46] and Berengut *et al.* [47] for astrophysically important transitions in C III. All values are here expressed in GHz u. The consistency with the NMS parameter is excellent for all transitions. The SMS parameters are in agreement with the non-relativistic calculations of Jönsson *et al.* as well as the values of Berengut *et al.* for the transition $1s^2 2s^2 \ ^1S_0 - 1s^2 2s2p \ ^3P_0^o$. Note however that our SMS parameter values grow with the J value, in contradiction with Berengut *et al.*'s results [47]. By summing the NMS and SMS contributions for the (13,12) and (14,12) isotopic pairs, the total mass shift values of Berengut *et al.*, $\delta\nu_{\text{MS}}^{13,12} = 28.76$ GHz and $\delta\nu_{\text{MS}}^{14,12} = 53.33$ GHz, are confirmed by our results (28.86 GHz and 53.51 GHz respectively). In their calculations, Berengut *et al.*, safely neglected the FS that we estimate to a few MHz.

Table 4 compares the wavenumber mass shifts calculated by Bubin *et al.* [48] using explicitly correlated Gaussian functions for the transition $1s^2 2s^2 \ ^1S_0 - 1s^2 2p^2 \ ^1S_0$ in C III with our results. Considering the high level of correlation included in [48], the almost perfect agreement between the two sets gives us confidence in our correlation models and computational strategy. The wavenumber field shifts have been estimated using (19) and taking the difference of the nuclear mean-square radii $\delta\langle r^2 \rangle^{13,12} = -0.044 \text{ fm}^2$ and $\delta\langle r^2 \rangle^{14,13} = 0.210 \text{ fm}^2$ from Angeli [44].

We report in table 5 our relativistic isotope shift parameters (K_{NMS} and K_{SMS}) for the ground state of beryllium-like ions B II-Ne VII and compare them with the non relativistic values obtained by King *et al.* [49] using a standard Hylleraas approach with Slater-type orbital (STO) basis functions, by Komasa *et al.* [50] using the explicitly correlated Gaussians approach, and by Galvez *et al.* [51] using the Monte Carlo algorithm, starting from explicitly correlated multideterminant wave functions. The one-body SMS parameters agree within 0.02% while the two-body SMS parameters do match within 0.4% for B II and 3% for Ne VII. For the density operator, the disagreement goes from 1% for B II to 4% for Ne VII. The comparison illustrates the importance of relativistic effects also for these ions.

To conclude this section on Be-like ions, we report in table 6 the $^{40,36}\text{Ar}$ isotope shift of the M1 intra-configuration transition $1s^2 2s 2p \ ^3P_1^o - ^3P_2^o$ in Ar^{14+} that has been measured by Orts *et al.* [52] using the electron beam ion trap at the Max-Planck-Institut für Kernphysik [52], and estimated theoretically in the same work [52], using the large-scale configuration interaction Dirac-Fock approach. As far as the MS is concerned, the consistency between the theoretical calculations is perfect. The experimental value is 5.3% smaller than the theoretical values that lie however within the experimental error bars. Our FS value is evaluated using the formula (19) and the difference of nuclear rms $\delta\langle r^2 \rangle^{40,36} = 0.2502 \text{ fm}^2$. It also shows a nice consistency with the evaluation of Orts *et al.* [52].

5.2. Boron-like ions

Table 7 displays the total and excitation energies, the \tilde{K}_{NMS} and \tilde{K}_{SMS} parameters as well as the electronic $\tilde{\mathcal{F}}$ field shift factors for several levels of B-like ions ($8 \leq Z \leq 30$ and $Z = 36, 42$). Table 8 compares the resulting $^{36,40}\text{Ar}^{13+}$ isotope shift of the $1s^2 2s^2 2p \ ^2P_{1/2}^o - ^2P_{3/2}^o$ forbidden line with the results of Tupitsyn *et al.* [16] and Orts *et al.* [52] using the large-scale RCI Dirac-Fock method to solve the Dirac-Coulomb-Breit equation. Their CSFs expansions were generated including “all single and double excitations and some part of triple excitations”. The nuclear charge distribution is described by a Fermi model and is therefore consistent with the present work. The upper part of the table shows the individual contributions of operators H_{NMS} and H_{SMS} to the wavenumber mass shift. A good agreement is observed between the two sets of values, the total wavenumber mass shift values differing by less than 0.8%. This example confirms the importance of the relativistic corrections to the recoil operator: the total wavenumber mass shift would indeed be 50% smaller if estimated from the uncorrected form of the mass Hamiltonian $\langle H_{\text{NMS}}^1 + H_{\text{SMS}}^1 \rangle$. The large cancellation of the terms involved in the transition isotope shift makes accurate calculations very challenging. For the sake of a fair comparison, the QED contributions (-0.0006 cm^{-1}) estimated by Orts *et al.* [52] have been subtracted from their theoretical estimation. The mass shifts values are extremely consistent. Orts *et al.* [52] also measured the transition IS at the Heidelberg electron beam ion trap with a satisfactory precision and the agreement observation-theory is rather good, as illustrated in table 8.

As an additional check of our RCI values at the neutral end of the isoelectronic sequence, we performed multiconfiguration Hartree-Fock (MCHF) calculations for O IV. The MCHF calculations are fully variational and the expansions obtained by SD-excitations from large MR sets to an active set of orbitals with $nl \leq 9h$. Results from these independent calculations are compared with the RCI values in table 9. The two different sets of specific mass shift parameters values differ by less than 1%, considering both the uncorrected term (K_{SMS}^1) or the corrected one (K_{SMS}). The two sets of calculations give specific mass shift parameters that on average differ by less than 0.4%, indicating that the uncertainties in the specific mass shift parameters from the present RCI calculations are very small.

5.3. Carbon-like ions

Table 10 displays the total and excitation energies, the \tilde{K}_{NMS} and \tilde{K}_{SMS} parameters as well as the electronic $\tilde{\mathcal{F}}$ field shift factors for several levels of C-like ions ($7 \leq Z \leq 28$). Table 11 presents the comparison with Jönsson and Bieroń's results [53] who calculated the uncorrected K_{SMS}^1 parameters. For each of the five ions considered in [53] (N II, O III, F IV, Ne V and Ti XVII), the K_{SMS}^1 values are compared with each other, and with the corrected K_{SMS} values evaluated in the present work (third column). The small difference between the K_{SMS}^1 values is due to differences in the optimization strategy. Furthermore, as generally observed [20, 31, 36], the relativistic corrections to the level specific mass shift barely reach a third of percent for light ions but reach 2% for Ti XVII. Jönsson and Bieroń observed that the SMS parameters for $2s2p^3\ ^3P^o$ and $2s2p^3\ ^1P^o$ approach each other for large Z . The present study extends the nuclear charges range considered and, as it can be seen from figure 1 that plots the differences of the SMS parameter values (ΔK_{SMS}) versus the nuclear charge for $^3P_{1,0}^o - ^1P_1^o$, the parameters indeed approach each other but this trend is not asymptotic. Some J -dependence appears: the sign of ΔK_{SMS} for $2s2p^3\ ^3P_0^o$ and $2s2p^3\ ^1P_1^o$ changes between $Z = 27$ and $Z = 28$, while for the transition $2s2p^3\ ^3P_1^o - ^1P_1^o$, the studied nuclear charges range of nuclear charges does not allow to observe the point where the ΔK_{SMS} cross the X -coordinate axis. Using a third degree polynomial extrapolation, the crossing is predicted to occur between $Z = 31$ and $Z = 32$. To further validate the present results, independent non relativistic SD-MR-MCHF calculations were performed for a few levels of O III. As it can be seen in table 12, the two sets of values agree very well, with an average difference 0.37% for K_{SMS}^1 , as expected for the neutral end of the isoelectronic sequence.

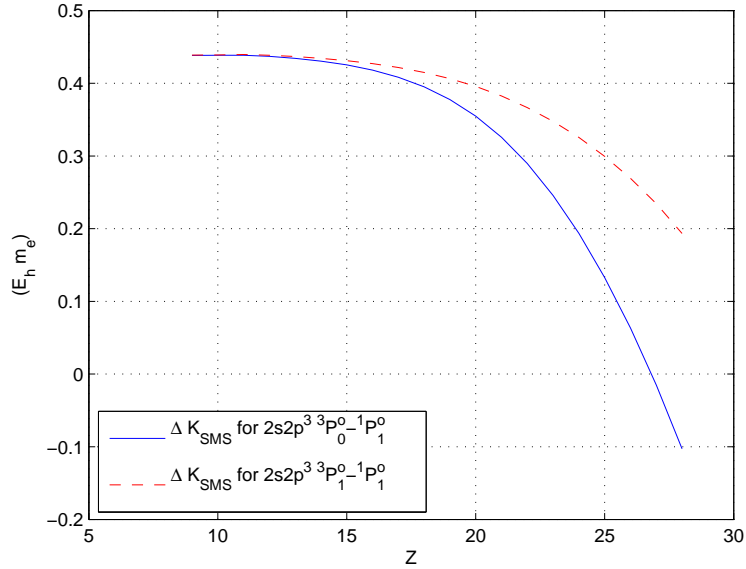


Fig. 1: Variation of the transition specific mass shift parameters along the isoelectronic sequence of C-like ions ($7 \leq Z \leq 28$) for $2s2p^3\ ^3P_0^o - ^1P_1^o$ (continuous blue line) and $2s2p^3\ ^3P_1^o - ^1P_1^o$ (dashed red line).

5.4. Nitrogen-like ions

Table 13 displays the total and excitation energies, the \tilde{K}_{NMS} and \tilde{K}_{SMS} parameters as well as the electronic $\tilde{\mathcal{F}}$ field shift factors for several levels for N-like ions ($8 \leq Z \leq 30$ and $Z = 36, 42$). To the knowledge of the authors, there are no isotope shift data to compare with along this sequence. To validate the current data independent SD-MR-MCHF calculations were performed for Ne IV. The comparison is presented in table 14, illustrating the good consistency between the two sets of results.

6. Outlook and conclusion

It is shown that relativistic configuration interaction calculations are capable of providing very accurate electronic isotope shift parameters for few-electron systems. The parameters are of value for interpreting current and future heavy-ion storage ring experiments and measurements on radioisotopes at ISOLDE to access changes in nuclear charge radii. However, it remains a true challenge to extend the current calculations to larger systems with a core. The fundamental problems are the large and canceling contributions to the mass shift from all core subshells. To obtain accurate results for the electronic mass shift parameters all electrons, even the ones deep down in the core, need to be correlated, leading to massive CSF expansions [54]. One way to handle these problems is to rely on divide and conquer strategies and divide the original large problem into a series of smaller ones for each pair of electrons that should be correlated. Contributions from all electron pairs are then put together at the end in one calculations that describes the full atomic system [55, 56]. Work along these lines are in progress [57].

Acknowledgments

Part of this work was supported by the Communauté française of Belgium (Action de Recherche Concertée), the Belgian National Fund for Scientific Research (FRFC/IISN Convention) and by the IUAP Belgian State Science Policy (BriX network P7/12). CN and SV are grateful to the “Fonds pour la formation la Recherche dans l’Industrie et dans l’Agriculture” of Belgium for a PhD grant (Boursier F.R.S.-FNRS). PJ gratefully acknowledges financial support from the Swedish Research Council (VR). PJ and GG acknowledges support from the Visby program of the Swedish Institute.

References

- [1] R. Kurucz, *Phys. Scr.* T47 (1993) 110.
- [2] R. Cayrel, M. Steffen, H. Chand, P. Bonifacio, M. Spite, F. Spite, P. Petitjean, H.-G. Ludwig, E. Caffau, *Astronomy & Astrophysics* 473 (2007) L37–L40.
- [3] C. Proffitt, P. Jönsson, U. Litzén, J. Pickering, G. Wahlgren, *Astrophys. J* 516 (1999) 342.
- [4] M. Lundqvist, G. M. Wahlgren, V. Hill, *Astronomy & Astrophysics* 463 (2007) 693–702.
- [5] I. U. Roederer, J. E. Lawler, J. S. Sobek, T. C. Beers, J. J. Cowan, A. Frebel, I. I. Ivans, H. Schatz, C. Sneden, I. B. Thompson, *The Astrophysical Journal Supplement Series* 203 (2012) 27.
- [6] M. G. Kozlov, V. A. Korol, J. C. Berengut, V. A. Dzuba, V. V. Flambaum, *Phys. Rev. A* 70 (2004) 062108.
- [7] J. C. Berengut, V. V. Flambaum, M. G. Kozlov, *J. Phys. B : At. Mol. Phys.* 41 (2008) 235702.
- [8] C. Brandau, C. Kozhuharov, Z. Harman, A. Müller, S. Schippers, Y. S. Kozhedub, D. Bernhardt, S. Böhm, J. Jacobi, E. W. Schmidt, P. H. Mokler, F. Bosch, H.-J. Kluge, T. Stöhlker, K. Beckert, P. Beller, F. Nolden, M. Steck, A. Gumberidze, R. Reuschl, U. Spillmann, F. J. Currell, I. I. Tupitsyn, V. M. Shabaev, U. D. Jentschura, C. H. Keitel, A. Wolf, Z. Stachura, *Phys. Rev. Lett.* 100 (2008) 073201.
- [9] W. Nörtershäuser, R. Sánchez, G. Ewald, A. Dax, J. Behr, P. Bricault, B. A. Bushaw, J. Dilling, M. Dombisky, G. W. F. Drake, S. Götte, H.-J. Kluge, T. Kühl, J. Lassen, C. D. P. Levy, K. Pachucki, M. Pearson, M. Puchalski, A. Wojtaszek, Z.-C. Yan, C. Zimmermann, *Phys. Rev. A* 83 (2011) 012516.
- [10] P. Cancio Pastor, L. Consolino, G. Giusfredi, P. De Natale, M. Inguscio, V. A. Yerokhin, K. Pachucki, *Phys. Rev. Lett.* 108 (2012) 143001.
- [11] M. Puchalski, D. Kędziera, K. Pachucki, *Phys. Rev. A* 87 (2013) 032503.
- [12] I. Angeli, K. Marinova, *Atomic Data and Nuclear Data Tables* 99 (2013) 69 – 95.
- [13] V. M. Shabaev, *Theor. and Mat. Phys.* 63 (1985) 588–596.
- [14] V. Shabaev, *Sov. J. Nucl. Phys.* 47 (1988) 69.
- [15] C. Palmer, *J. Phys. B : At. Mol. Phys.* 20 (1987) 5987–5996.
- [16] I. I. Tupitsyn, V. M. Shabaev, J. R. C. López-Urrutia, I. Draganic, R. S. Orts, J. Ullrich, *Phys. Rev. A* 68 (2003) 022511.
- [17] V. A. Korol, M. G. Kozlov, *Phys. Rev. A* 76 (2007) 022103–7.
- [18] Y. S. Kozhedub, O. V. Andreev, V. M. Shabaev, I. I. Tupitsyn, C. Brandau, C. Kozhuharov, G. Plunien, T. Stöhlker, *Phys. Rev. A* 77 (2008) 032501.
- [19] S. G. Porsev, M. G. Kozlov, D. Reimers, *Phys. Rev. A* 79 (2009) 032519.
- [20] Y. S. Kozhedub, A. V. Volotka, A. N. Artemyev, D. A. Glazov, G. Plunien, V. M. Shabaev, I. I. Tupitsyn, T. Stöhlker, *Phys. Rev. A* 81 (2010) 042513.
- [21] T. J. Procter, J. Billowes, M. L. Bissell, K. Blaum, F. C. Charlwood, B. Cheal, K. T. Flanagan, D. H. Forest,

- S. Fritzsche, C. Geppert, H. Heylen, M. Kowalska, K. Kreim, A. Krieger, J. Krämer, K. M. Lynch, E. Mané, I. D. Moore, R. Neugart, G. Neyens, W. Nörtershäuser, J. Papuga, M. M. Rajabali, H. H. Stroke, P. Vingerhoets, D. T. Yordanov, M. Žáková, *Phys. Rev. C* 86 (2012) 034329.
- [22] B. Cheal, T. E. Cocolios, S. Fritzsche, *Phys. Rev. A* 86 (2012) 042501.
- [23] S. Schippers, *Journal of Physics: Conference Series* 163 (2009) 012001.
- [24] S. Schippers, *Journal of Physics: Conference Series* 388 (2012) 012010.
- [25] M. Grieser, Y. A. Litvinov, R. Raabe, K. Blaum, Y. Blumenfeld, P. A. Butler, F. Wenander, W. *et al.* (123 more), *The European Physical Journal Special Topics* 207 (2012) 1–117.
- [26] P. Jönsson, X. He, C. Froese Fischer, I. Grant, *Comput. Phys. Commun.* 177 (2007) 597–622.
- [27] P. Jönsson, G. Gaigalas, J. Bieroń, C. Froese Fischer, I. Grant, *Comput. Phys. Commun.* 184 (2013) 2197.
- [28] C. Nazé, E. Gaidamauskas, G. Gaigalas, M. Godefroid, P. Jönsson, *Computer Physics Communications* 184 (2013) 2187.
- [29] S. Blundell, P. Baird, C. Palmer, D. Stacey, G. Woodgate, *J. Phys. B : At. Mol. Phys.* 20 (1987) 3663–3681.
- [30] V. Shabaev, A. Artemyev, *J. Phys. B : At. Mol. Phys.* 27 (1994) 1307–1314.
- [31] E. Gaidamauskas, C. Nazé, P. Rynkun, G. Gaigalas, P. Jönsson, M. Godefroid, *Journal of Physics B: Atomic, Molecular and Optical Physics* 44 (2011) 175003.
- [32] G. Torbohm, B. Fricke, A. Rosén, *Phys. Rev. A* 31 (1985) 2038–2053.
- [33] G. Fricke, C. Bernhardt, K. Heilig, L. Schaller, L. Schellenberg, E. Shera, C. De Jager, *At. Data Nucl. Data Tables* 60 (1995) 177–285.
- [34] I. Grant, *Relativistic Quantum Theory of Atoms and Molecules. Theory and Computation, Atomic, Optical and Plasma Physics*, Springer, New York, USA, 2007.
- [35] F. A. Parpia, A. K. Mohanty, *Phys. Rev. A* 46 (1992) 3735–3745.
- [36] J. Li, C. Nazé, M. Godefroid, S. Fritzsche, G. Gaigalas, P. Indelicato, P. Jönsson, *Phys. Rev. A* 86 (2012) 022518.
- [37] K. Dylla, I. Grant, C. Johnson, F. Parpia, E. Plummer, *Computer Physics Communications* 55 (1989) 425 – 456.
- [38] L. Stuesson, P. Jönsson, C. Froese Fischer, *Computer Physics Communications* 177 (2007) 539 – 550.
- [39] P. Rynkun, P. Jönsson, G. Gaigalas, C. Froese Fischer, *At. Data Nucl. Data Tables* 98 (2012) 481–556.
- [40] P. Jönsson, P. Rynkun, G. Gaigalas, *Atomic Data and Nuclear Data Tables* 97 (2011) 648 – 691.
- [41] P. Rynkun, P. Jönsson, G. Gaigalas, C. Froese Fischer, *Atomic Data and Nuclear Data Tables* (2013).
- [42] U. Litzén, T. Zethson, P. Jönsson, J. Kasten, R. Kling, F. Launay, *Phys. Rev. A* 57 (1998) 2477–2484.
- [43] C. Froese Fischer, G. Tachiev, G. Gaigalas, M. Godefroid, *Comput. Phys. Commun.* 176 (2007) 559–579.
- [44] I. Angeli, *At. Data Nucl. Data Tables* 87 (2004) 185–206.
- [45] S. R. Federman, D. L. Lambert, J. A. Cardelli, Y. Sheffer, *Nature* 381 (1996) 764–766.

- [46] P. Jönsson, C. Froese Fischer, M. Godefroid, *J. Phys. B : At. Mol. Phys.* 32 (1999) 1233–1245.
- [47] J. C. Berengut, V. V. Flambaum, M. G. Kozlov, *Phys. Rev. A* 73 (2006) 012504.
- [48] S. Bubin, J. Komasa, M. Stanke, L. Adamowicz, *Phys. Rev. A* 81 (2010) 052504.
- [49] F. W. King, D. Quicker, J. Langer, *The Journal of Chemical Physics* 134 (2011) 124114.
- [50] J. Komasa, J. Rychlewski, K. Jankowski, *Phys. Rev. A* 65 (2002) 042507.
- [51] F. J. Gálvez, E. Buendia, A. Sarsa, *The Journal of Chemical Physics* 111 (1999) 10903–10909.
- [52] R. S. Orts, Z. Harman, J. R. C. López-Urrutia, A. N. Artemyev, H. Bruhns, A. J. G. Martínez, U. D. Jentschura, C. H. Keitel, A. Lapierre, V. Mironov, V. M. Shabaev, H. Tawara, I. I. Tupitsyn, J. Ullrich, A. V. Volotka, *Phys. Rev. Lett.* 97 (2006) 103002.
- [53] P. Jönsson, J. Bieroń, *Journal of Physics B: Atomic, Molecular and Optical Physics* 43 (2010) 074023.
- [54] C. Froese Fischer, P. Jönsson, M. Godefroid, *Phys. Rev. A* 57 (1998) 1753–1758.
- [55] S. Verdebout, P. Rynkun, P. Jönsson, G. Gaigalas, C. Froese Fischer, M. Godefroid, *Journal of Physics B: Atomic, Molecular and Optical Physics* 46 (2013) 085003.
- [56] C. Froese Fischer, S. Verdebout, M. Godefroid, P. Rynkun, P. Jönsson, G. Gaigalas, *Phys. Rev. A* (2013) in press.
- [57] M. Godefroid, P. Jönsson, G. Gaigalas (2013). Work in progress.
- [58] P. Jönsson, S. G. Johansson, C. F. Fischer, *Astrophysical Journal Letters* 429 (1994) L45–L48.

Explanation of Tables

Table 1. Total energies (in E_h), excitation energies (in cm^{-1}), normal and specific mass shift \widetilde{K} parameters (in GHz u), $\widetilde{\mathcal{F}}$ field shift factors (in GHz/ fm^2) for levels in the beryllium isoelectronic sequence ($5 \leq Z \leq 74$). For each of the many-electron wave functions, the leading components are given in the LSJ coupling scheme. The number in square brackets is the power of 10.

Level composition in LSJ coupling	Leading components expressed within the LSJ coupling scheme for each calculated level.
Energy	The calculated total energy in atomic units (E_h).
ΔE	Calculated energy relative to the ground state (in cm^{-1}).
$\widetilde{K}_{\text{NMS}} = K_{\text{NMS}}/h$	The normal mass shift parameter in GHz u (see eq.(6)).
$\widetilde{K}_{\text{SMS}} = K_{\text{SMS}}/h$	The specific mass shift parameter in GHz u (see eq.(7)).
$\widetilde{\mathcal{F}}$	The electronic field shift factor in GHz/ fm^2 (see eq.(13)).

Table 2. Comparison of wavenumber isotope shifts $\delta\sigma$ (in cm^{-1}) for several transitions in B II between the isotopes ^{11}B and ^{10}B .

Exp. $\delta\sigma_{\text{IS}}$	Experimental transition IS (in cm^{-1})
$\delta\sigma_{\text{MS}}$	Transition mass shift (in cm^{-1}).
$\delta\sigma_{\text{FS}}$	Transition field shift (in cm^{-1}) (see eq.(19)).

Table 3. Comparison of the $\Delta\widetilde{K}_{\text{NMS}}$ and $\Delta\widetilde{K}_{\text{SMS}}$ parameters (in GHz u) with previous theoretical works for several transitions in C III.

$\Delta\widetilde{K}_{\text{NMS}}$	Transition normal mass shift (NMS) parameters (in GHz u).
$\Delta\widetilde{K}_{\text{SMS}}$	Transition specific mass shift (SMS) parameters (in GHz u).

Table 4. Wavenumber mass shift $\delta\sigma_{\text{MS}}$ and field shift $\delta\sigma_{\text{FS}}$ (in cm^{-1}) for the transition $1s^22s^2\ ^1S_0 - 1s^22p^2\ ^1S_0$ in C^{2+} ion for the isotope pairs ^{13}C - ^{12}C and ^{14}C - ^{13}C .

$\delta\sigma_{\text{MS}}$	Transition mass shift (in cm^{-1}).
$\delta\sigma_{\text{FS}}$	Transition field shift (in cm^{-1}).

Table 5. Comparative table of the expectation values of our isotope shift parameters (in a.u.) with calculations based on Hylleraas wave functions for some ions at the neutral end of the Be-like sequence.

K_{NMS}	Level normal mass shift parameter (see eq.(6)) calculated with the one-body part of (4).
$\langle -\frac{1}{2}\nabla_i^2 \rangle$	Non relativistic kinetic energy.
K_{SMS}	Level specific mass shift parameter (see eq.(7)) calculated with the two-body part of (4).
$\rho^e(\mathbf{0})$	Total probability density at the origin estimated from eq.(14).
$\langle \delta(\mathbf{r}_i) \rangle$	Non relativistic total probability density at the origin (nuclear point charge).

Table 6. Wavenumber mass shift $\delta\sigma_{\text{MS}}$ and field shift $\delta\sigma_{\text{FS}}$ (in cm^{-1}) for the $1s^22s2p\ ^3P_1^o - ^3P_2^o$ in Ar^{14+} for the isotope pair $^{40,36}\text{Ar}$.

Same as for Table 4.

Table 7. Total energies (in E_{h}), excitation energies (in cm^{-1}), normal and specific mass shift \widetilde{K} parameters (in GHz u), $\widetilde{\mathcal{F}}$ field shift factors (in GHz/ fm^2) for levels in the boron isoelectronic sequence ($8 \leq Z \leq 30$ and $Z = 36, 42$). For each of the many-electron wave functions, the leading components are given in the LSJ coupling scheme. The number in square brackets is the power of 10.

Same as for Table 1.

Table 8. Upper part: individual contributions to the wavenumber mass shift $\delta\sigma_{\text{MS}}$ of the forbidden transition $1s^22s^2\ 2p\ ^2P_{1/2}^o - ^2P_{3/2}^o$ in boron-like $^{36,40}\text{Ar}^{13+}$. Lower part: wavenumber mass, field and total shifts. (All numbers in cm^{-1}).

$\langle H_{\text{NMS}}^i \rangle$ ($i = 1, 2, 3$)	Normal mass shift (one-body) contributions from the three terms of eq.(4).
$\langle H_{\text{SMS}}^i \rangle$ ($i = 1, 2, 3$)	Specific mass shift (two-body) contributions from the three terms of eq.(4).
$\delta\sigma_{\text{MS}}$	Transition mass shift (in cm^{-1}).
$\delta\sigma_{\text{FS}}$	Transition field shift (in cm^{-1}).
$\delta\sigma$	Total transition isotope shift (in cm^{-1}).

Table 9. Comparison of MCHF and MCDHF specific mass shift parameters for O IV (all values in atomic units $E_{\text{h}}m_e$).

MCHF K_{SMS}^1	Non relativistic specific mass shift parameter.
MCDHF K_{SMS}^1	Relativistic specific mass shift parameter calculated with $\frac{1}{2}\langle\sum_{i\neq j}^N (\mathbf{p}_i \cdot \mathbf{p}_j)\rangle$.
MCDHF K_{SMS}	Relativistic specific mass shift parameter calculated with the two-body part of the relativistic recoil operator (4).

Table 10. Total energies (in E_{h}), excitation energies (in cm^{-1}), normal and specific mass shift \widetilde{K} parameters (in GHz u), $\widetilde{\mathcal{F}}$ field shift factors (in GHz/ fm^2) for levels in the carbon isoelectronic sequence ($7 \leq Z \leq 28$). For each of the many-electron wave functions, the leading components are given in the LSJ coupling scheme. The number in square brackets is the power of 10.

Same as for Table 1.

Table 11. Comparison of corrected (K_{SMS}) and uncorrected (K_{SMS}^1) specific shift parameters (in $E_{\text{h}}m_e$) for several states of N II, O III, F IV, Ne V and Ti XVII.

K_{SMS}^1	Relativistic specific mass shift parameter calculated with $\frac{1}{2}\langle\sum_{i\neq j}^N (\mathbf{p}_i \cdot \mathbf{p}_j)\rangle$.
K_{SMS}	Relativistic specific mass shift parameter calculated with the two-body part of the relativistic recoil operator (4).

Table 12. Comparison of MCHF and MCDHF specific mass shift parameters for O III (in atomic units $E_h m_e$).

Same as for Table 9.

Table 13. Total energies (in E_h), excitation energies (in cm^{-1}), normal and specific mass shift \tilde{K} parameters (in GHz u), $\tilde{\mathcal{F}}$ field shift factors (in GHz/fm²) for levels in the nitrogen isoelectronic sequence ($7 \leq Z \leq 36$ and $Z = 42, 74$). For each of the many-electron wave functions, the leading components are given in the *LSJ* coupling scheme. The number in square brackets is the power of 10.

Same as for Table 1.

Table 14. Comparison of MCHF and MCDHF specific mass shift parameters for Ne IV (in atomic units $E_h m_e$).

Same as for Table 9.

Table 1

Total energies (in E_h), excitation energies (in cm^{-1}), normal and specific mass shift \tilde{K} parameters (in GHz u), \tilde{F} field shift factors (in GHz/fm²) for levels in the beryllium isoelectronic sequence ($5 \leq Z \leq 74$). For each of the many-electron wave functions, the leading components are given in the LSJ coupling scheme. The number in square brackets is the power of 10. See page 16 for Explanation of Tables.

Level composition in LSJ coupling		J	Energy (E_h)	ΔE (cm^{-1})	\tilde{K}_{NMS} (GHz u)	\tilde{K}_{SMS} (GHz u)	\tilde{F} (GHz/fm ²)	
B II								
$1s^2 2s^2 \ ^1S$	(92%) + $1s^2 2p^2 \ ^1S$	(7%)	0	-24.3534464	0.00	8.7862981[4]	2.1587130[3]	1.803445
$1s^2 2s 2p \ ^3P^o$	(99%)		0	-24.1836233	37271.86	8.7249235[4]	3.1895258[2]	1.763953
	(99%)		1	-24.1835957	37277.92	8.7249488[4]	3.1855676[2]	1.763955
	(99%)		2	-24.1835226	37293.97	8.7249802[4]	3.1780709[2]	1.763958
$1s^2 2s 2p \ ^1P^o$	(96%) + $1s^2 2p 3d \ ^1P^o$	(3%)	1	-24.0185813	73494.38	8.6679944[4]	9.8372368[2]	1.759018
$1s^2 2p^2 \ ^3P$	(99%)		0	-23.9028711	98889.85	8.6233220[4]	-1.1484849[3]	1.715645
	(99%)		1	-23.9028320	98898.43	8.6233347[4]	-1.1488285[3]	1.715646
	(99%)		2	-23.9027712	98911.77	8.6233776[4]	-1.1496300[3]	1.715647
$1s^2 2p^2 \ ^1D$	(93%) + $1s^2 2s 3d \ ^1D$	(6%)	2	-23.8868692	102401.85	8.6187672[4]	-1.4767884[3]	1.720387
$1s^2 2p^2 \ ^1S$	(65%) + $1s^2 2s n s \ ^1S$	(21%)	0	-23.7723539	127540.87	8.5772099[4]	4.4681013[2]	1.735702
C III								
$1s^2 2s^2 \ ^1S$	(93%) + $1s^2 2p^2 \ ^1S$	(7%)	0	-36.5465996	0.00	1.3183511[5]	2.5919811[3]	3.882932
$1s^2 2s 2p \ ^3P^o$	(100%)		0	-36.3082037	52321.84	1.3097505[5]	-8.8188170[2]	3.778061
	(100%)		1	-36.3080969	52345.30	1.3097551[5]	-8.8287835[2]	3.778068
	(100%)		2	-36.3078401	52401.66	1.3097597[5]	-8.8477109[2]	3.778077
$1s^2 2s 2p \ ^1P^o$	(98%) + $1s^2 2p 3d \ ^1P^o$	(2%)	1	-36.0796648	102480.34	1.3017542[5]	-2.3422019[2]	3.763878
$1s^2 2p^2 \ ^3P$	(100%)		0	-35.9204369	137426.82	1.2957660[5]	-4.0261275[3]	3.652846
	(100%)		1	-35.9203054	137455.69	1.2957679[5]	-4.0269916[3]	3.652848
	(100%)		2	-35.9200881	137503.37	1.2957764[5]	-4.0290930[3]	3.652852
$1s^2 2p^2 \ ^1D$	(97%) + $1s^2 2s 3d \ ^1D$	(3%)	2	-35.8815892	145952.90	1.2944282[5]	-4.3692705[3]	3.658962
$1s^2 2p^2 \ ^1S$	(90%) + $1s^2 2s^2 \ ^1S$	(7%)	0	-35.7133814	182870.26	1.2886470[5]	-2.5924073[3]	3.666821
N IV								
$1s^2 2s^2 \ ^1S$	(93%) + $1s^2 2p^2 \ ^1S$	(7%)	0	-51.2469981	0.00	1.8483436[5]	2.9718617[3]	7.407165
$1s^2 2s 2p \ ^3P^o$	(100%)		0	-50.9409665	67166.16	1.8372581[5]	-2.6458384[3]	7.179712
	(100%)		1	-50.9406808	67228.87	1.8372636[5]	-2.6478501[3]	7.179727
	(100%)		2	-50.9400241	67373.00	1.8372659[5]	-2.6516780[3]	7.179748
$1s^2 2s 2p \ ^1P^o$	(98%) + $1s^2 2p 3d \ ^1P^o$	(1%)	1	-50.6507583	130859.51	1.8271848[5]	-2.0338715[3]	7.150993
$1s^2 2p^2 \ ^3P$	(100%)		0	-50.4471847	175538.75	1.8194605[5]	-8.0577165[3]	6.912282
	(100%)		1	-50.4468509	175612.01	1.8194617[5]	-8.0595122[3]	6.912285
	(100%)		2	-50.4462839	175736.44	1.8194736[5]	-8.0638219[3]	6.912289
$1s^2 2p^2 \ ^1D$	(98%) + $1s^2 2s 3d \ ^1D$	(2%)	2	-50.3859686	188974.12	1.8173659[5]	-8.3978922[3]	6.920357
$1s^2 2p^2 \ ^1S$	(92%) + $1s^2 2s^2 \ ^1S$	(7%)	0	-50.1729720	235721.48	1.8100420[5]	-6.0531219[3]	6.939223
O V								
$1s^2 2s^2 \ ^1S$	(93%) + $1s^2 2p^2 \ ^1S$	(6%)	0	-68.4561090	0.00	2.4685524[5]	3.3000756[3]	1.294328[1]
$1s^2 2s 2p \ ^3P^o$	(100%)		0	-68.0829532	81898.22	2.4550519[5]	-4.9699967[3]	1.251036[1]
	(100%)		1	-68.0823306	82034.87	2.4550578[5]	-4.9736495[3]	1.251038[1]
	(100%)		2	-68.0809356	82341.03	2.4550546[5]	-4.9806273[3]	1.251041[1]
$1s^2 2s 2p \ ^1P^o$	(99%) + $1s^2 2p 3d \ ^1P^o$	(1%)	1	-67.7318850	158948.79	2.4426731[5]	-4.3845899[3]	1.246101[1]
$1s^2 2p^2 \ ^3P$	(100%)		0	-67.4835066	213461.55	2.4333869[5]	-1.3224214[4]	1.200656[1]
	(100%)		1	-67.4827968	213617.33	2.4333843[5]	-1.3227540[4]	1.200656[1]
	(100%)		2	-67.4815738	213885.75	2.4333961[5]	-1.3235270[4]	1.200655[1]
$1s^2 2p^2 \ ^1D$	(99%) + $1s^2 2s 3d \ ^1D$	(1%)	2	-67.3998597	231819.91	2.4305754[5]	-1.3558633[4]	1.201700[1]
$1s^2 2p^2 \ ^1S$	(92%) + $1s^2 2s^2 \ ^1S$	(6%)	0	-67.1427354	288252.17	2.4217376[5]	-1.0576225[4]	1.205516[1]
F VI								
$1s^2 2s^2 \ ^1S$	(94%) + $1s^2 2p^2 \ ^1S$	(6%)	0	-88.1763150	0.00	3.1789787[5]	3.5780144[3]	2.116740[1]
$1s^2 2s 2p \ ^3P^o$	(100%)		0	-87.7363221	96567.28	3.1630501[5]	-7.8504163[3]	2.041521[1]
	(100%)		1	-87.7351344	96827.94	3.1630520[5]	-7.8564175[3]	2.041524[1]
	(100%)		2	-87.7325093	97404.10	3.1630322[5]	-7.8679642[3]	2.041527[1]
$1s^2 2s 2p \ ^1P^o$	(99%)		1	-87.3242038	187016.78	3.1485170[5]	-7.2977739[3]	2.033782[1]
$1s^2 2p^2 \ ^3P$	(100%)		0	-87.0310434	251358.06	3.1375479[5]	-1.9515690[4]	1.954584[1]
	(100%)		1	-87.0297018	251652.50	3.1375368[5]	-1.9521455[4]	1.954581[1]
	(100%)		2	-87.0273805	252161.97	3.1375420[5]	-1.9534147[4]	1.954578[1]
$1s^2 2p^2 \ ^1D$	(99%) + $1s^2 2s 3d \ ^1D$	(1%)	2	-86.9246298	274713.15	3.1339951[5]	-1.9843945[4]	1.955904[1]
$1s^2 2p^2 \ ^1S$	(93%) + $1s^2 2s^2 \ ^1S$	(6%)	0	-86.6234869	340806.36	3.1237073[5]	-1.6178494[4]	1.962795[1]
Ne VII								
$1s^2 2s^2 \ ^1S$	(94%) + $1s^2 2p^2 \ ^1S$	(6%)	0	-110.4104945	0.00	3.9796222[5]	3.8077957[3]	3.287145[1]
$1s^2 2s 2p \ ^3P^o$	(100%)		0	-109.9037877	111209.28	3.9612528[5]	-1.1284298[4]	3.164860[1]
	(100%)		1	-109.9017247	111662.06	3.9612449[5]	-1.1293534[4]	3.164864[1]
	(100%)		2	-109.8971979	112655.56	3.9611933[5]	-1.1311504[4]	3.164863[1]
$1s^2 2s 2p \ ^1P^o$	(99%)		1	-109.4302639	215135.73	3.9445683[5]	-1.0765963[4]	3.153449[1]
$1s^2 2p^2 \ ^3P$	(100%)		0	-109.0921768	289337.28	3.9319099[5]	-2.6924418[4]	3.024295[1]
	(100%)		1	-109.0898452	289848.99	3.9318825[5]	-2.6933969[4]	3.024285[1]

Continued...

Table 1 (continued)

Level composition in LSJ coupling				J	Energy (E_h)	ΔE (cm^{-1})	\tilde{K}_{NMS} (GHz u)	\tilde{K}_{SMS} (GHz u)	\tilde{F} (GHz/fm ²)
$1s^2 2p^2 \ ^3P$	(100%)			1	-6616.1916040	13226584.18	2.2010767[7]	-2.1340665[6]	3.304671[5]
$1s^2 2p^2 \ ^1D$	(65%)	+ $1s^2 2p^2 \ ^3P$	(35%)	2	-6615.5376180	13370117.51	2.2010741[7]	-2.1377706[6]	3.304686[5]
$1s^2 2p^2 \ ^3P$	(65%)	+ $1s^2 2p^2 \ ^1D$	(35%)	2	-6570.6354568	23225002.50	2.1867258[7]	-2.2864217[6]	3.292049[5]
$1s^2 2p^2 \ ^1S$	(68%)	+ $1s^2 2p^2 \ ^3P$	(31%)	0	-6568.2515039	23748219.67	2.1856951[7]	-2.2673029[6]	3.292437[5]
Hf LXIX									
$1s^2 2s^2 \ ^1S$	(98%)	+ $1s^2 2p^2 \ ^1S$	(1%)	0	-6884.3911633	0.00	2.2782062[7]	2.5196394[4]	4.152603[5]
$1s^2 2s2p \ ^3P^o$	(100%)			0	-6878.3802008	1319253.76	2.2779869[7]	-9.8338063[5]	3.901188[5]
	(71%)	+ $1s^2 2s2p \ ^1P^o$	(29%)	1	-6877.1773115	1583257.44	2.2777083[7]	-9.8632355[5]	3.900439[5]
$1s^2 2p^2 \ ^3P$	(68%)	+ $1s^2 2p^2 \ ^1S$	(31%)	0	-6867.3631138	3737224.79	2.2758466[7]	-1.9741067[6]	3.647153[5]
$1s^2 2s2p \ ^3P^o$	(100%)			2	-6830.3089193	11869680.23	2.2628187[7]	-1.1647112[6]	3.887217[5]
$1s^2 2s2p \ ^1P^o$	(71%)	+ $1s^2 2s2p \ ^3P^o$	(29%)	1	-6827.1067834	12572467.81	2.2617291[7]	-1.1411245[6]	3.885195[5]
$1s^2 2p^2 \ ^3P$	(100%)			1	-6820.8271405	13950690.07	2.2611926[7]	-2.1781965[6]	3.624356[5]
$1s^2 2p^2 \ ^1D$	(65%)	+ $1s^2 2p^2 \ ^3P$	(35%)	2	-6820.1714727	14094592.52	2.2611989[7]	-2.1820600[6]	3.624372[5]
$1s^2 2p^2 \ ^3P$	(65%)	+ $1s^2 2p^2 \ ^1D$	(35%)	2	-6772.3142638	24598035.50	2.2459204[7]	-2.3436363[6]	3.609892[5]
$1s^2 2p^2 \ ^1S$	(68%)	+ $1s^2 2p^2 \ ^3P$	(32%)	0	-6769.8896780	25130170.57	2.2448676[7]	-2.3243054[6]	3.610286[5]
Ta LXX									
$1s^2 2s^2 \ ^1S$	(98%)	+ $1s^2 2p^2 \ ^1S$	(1%)	0	-7096.4159449	0.00	2.3394747[7]	2.5855312[4]	4.566694[5]
$1s^2 2s2p \ ^3P^o$	(100%)			0	-7090.2614411	1350757.42	2.3395816[7]	-1.0006638[6]	4.289498[5]
	(70%)	+ $1s^2 2s2p \ ^1P^o$	(30%)	1	-7089.0410978	1618591.81	2.3393044[7]	-1.0038244[6]	4.288679[5]
$1s^2 2p^2 \ ^3P$	(68%)	+ $1s^2 2p^2 \ ^1S$	(31%)	0	-7078.9984941	3822688.48	2.3375735[7]	-2.0029768[6]	4.008140[5]
$1s^2 2s2p \ ^3P^o$	(100%)			2	-7039.0845004	12582797.28	2.3234754[7]	-1.1975095[6]	4.273585[5]
$1s^2 2s2p \ ^1P^o$	(70%)	+ $1s^2 2s2p \ ^3P^o$	(30%)	1	-7035.8274523	13297636.70	2.3223767[7]	-1.1719616[6]	4.271390[5]
$1s^2 2p^2 \ ^3P$	(100%)			1	-7029.3861295	14711343.59	2.3219705[7]	-2.2213846[6]	3.982420[5]
$1s^2 2p^2 \ ^1D$	(65%)	+ $1s^2 2p^2 \ ^3P$	(35%)	2	-7028.7291971	14855523.59	2.3219864[7]	-2.2254117[6]	3.982438[5]
$1s^2 2p^2 \ ^3P$	(65%)	+ $1s^2 2p^2 \ ^1D$	(35%)	2	-6977.7589077	26042208.75	2.3057302[7]	-2.4009660[6]	3.965819[5]
$1s^2 2p^2 \ ^1S$	(68%)	+ $1s^2 2p^2 \ ^3P$	(32%)	0	-6975.2931347	26583383.36	2.3046550[7]	-2.3814115[6]	3.966221[5]
W LXXI									
$1s^2 2s2p \ ^3P^o$	(100%)			0	-7318.5525559	0.00	2.4014284[7]	-1.0147471[6]	4.709503[5]
	(70%)	+ $1s^2 2s2p \ ^1P^o$	(30%)	1	-7317.3151885	271570.75	2.4011502[7]	-1.0181653[6]	4.708617[5]
$1s^2 2s^2 \ ^1S$	(98%)	+ $1s^2 2p^2 \ ^1S$	(1%)	0	-7312.5628230	1314594.38	2.4010095[7]	2.6522076[4]	5.015326[5]
$1s^2 2p^2 \ ^3P$	(67%)	+ $1s^2 2p^2 \ ^1S$	(31%)	0	-7294.7502196	5224008.84	2.3996578[7]	-2.0296947[6]	4.398914[5]
$1s^2 2s2p \ ^3P^o$	(100%)			2	-7264.1537164	11939164.91	2.3843161[7]	-1.2285076[6]	4.691287[5]
$1s^2 2s2p \ ^1P^o$	(70%)	+ $1s^2 2s2p \ ^3P^o$	(30%)	1	-7260.8409814	12666226.18	2.3831983[7]	-1.2008271[6]	4.688914[5]
$1s^2 2p^2 \ ^3P$	(100%)			1	-7241.8978000	16823773.81	2.3830608[7]	-2.2635132[6]	4.369924[5]
$1s^2 2p^2 \ ^1D$	(65%)	+ $1s^2 2p^2 \ ^3P$	(35%)	2	-7241.2400286	16968137.93	2.3830864[7]	-2.2677077[6]	4.369944[5]
$1s^2 2p^2 \ ^3P$	(65%)	+ $1s^2 2p^2 \ ^1D$	(35%)	2	-7186.9916243	28874286.14	2.3658052[7]	-2.4583792[6]	4.350899[5]
$1s^2 2p^2 \ ^1S$	(68%)	+ $1s^2 2p^2 \ ^3P$	(32%)	0	-7184.4841007	29424623.94	2.3647071[7]	-2.4385888[6]	4.351310[5]

Table 2

Comparison with other works (experiment and theory) of wavenumber isotope shifts $\delta\sigma$ (in cm^{-1}) for several transitions in B II between the isotopes ^{11}B and ^{10}B .

	Exp.	Theory	This work	
	$\delta\sigma_{\text{IS}}$	$\delta\sigma_{\text{MS}}$	$\delta\sigma_{\text{MS}}$	$\delta\sigma_{\text{FS}}$
$2s^2 \ ^1S_0 - 2s2p \ ^1P_1^o$	0.70 ^a	0.7145 ^a	0.711	0.00016
	0.74(19) ^b	0.7146 ^c		
		0.7165 ^d		
$2s2p \ ^3P_1^o - 2p^2 \ ^3P_2$	0.80(4) ^a	0.7485 ^a	0.749	-0.00017
$2s2p \ ^1P_1^o - 2p^2 \ ^1S_0$	0.419 ^a	0.4263 ^a	0.478	-0.00010
$2s2p \ ^1P_1^o - 2p^2 \ ^1D_2$	0.887 ^a	0.8870 ^a	0.890	-0.00014

^a Litzén *et al.* [42]

^b Astronomical observations from Federman *et al.* [45]

^c Jönsson *et al.* [46]

^d MCHF calculations of Jönsson *et al.* [58] - no limits on orbital quantum numbers.

Table 3

Comparison of the $\Delta\tilde{K}_{\text{NMS}}$ and $\Delta\tilde{K}_{\text{SMS}}$ parameters (in GHz u) with previous theoretical works for several transitions in C III.

	$\Delta\tilde{K}_{\text{NMS}}$		$\Delta\tilde{K}_{\text{SMS}}$	
	Other works	This work	Other works	This work
$2s^2\ ^1S - 2s2p\ ^3P^o$			-3475^c	
$2s^2\ ^1S_0 - 2s2p\ ^3P_0^o$	-860.3^a	-860.1	$-3453(7)^a$	-3474
			-3473^b	
$2s^2\ ^1S_0 - 2s2p\ ^3P_1^o$	-860.2^a	-859.8	$-3454(7)^a$	-3475
			-3472^b	
$2s^2\ ^1S_0 - 2s2p\ ^3P_2^o$	-860.1^a	-859.4	$-3454(7)^a$	-3477
			-3468^b	
$2s^2\ ^1S - 2s2p\ ^1P^o$			-2817^c	
$2s^2\ ^1S_0 - 2s2p\ ^1P_1^o$	-1677.3^a	-1660	$-2774(80)^a$	-2826
			-2790^b	

^aKorol and Kozlov [17]

^bBerengut *et al.* [47]

^cJönsson *et al.* [46]

Table 4

Wavenumber mass shift $\delta\sigma_{\text{MS}}$ and field shift $\delta\sigma_{\text{FS}}$ (in cm^{-1}) for the transition $1s^22s^2\ ^1S_0 - 1s^22p^2\ ^1S_0$ in C^{2+} ion for the isotope pairs ^{13}C - ^{12}C and ^{14}C - ^{13}C .

	$\delta\sigma_{\text{MS}}^{13,12}$	$\delta\sigma_{\text{FS}}^{13,12}$	$\delta\sigma_{\text{MS}}^{14,13}$	$\delta\sigma_{\text{FS}}^{14,13}$
This work	1.750	0.00032	1.493	-0.00151
Bubin <i>et al.</i> [48]	1.755		1.498	

Table 5

Comparison of the electronic isotope shift parameters with previous non-relativistic works for the ground states of beryllium-like B II - Ne VII.

	B II	C III	N IV
K_{NMS}	24.3423 ^a	36.5247 ^a	51.2080 ^a
$\langle -\frac{1}{2}\nabla_i^2 \rangle$	24.34878 ^b	36.53446 ^b	51.22221 ^b
K_{SMS}	0.5981 ^a	0.7181 ^a	0.8233 ^a
$-\langle \nabla_i \cdot \nabla_j \rangle$	0.59554(40) ^b	0.71314(50) ^b	0.81569(50) ^b
	0.595140 ^c	0.713671 ^c	0.816044 ^c
$\rho^e(\mathbf{0})$	73.29451 ^a	131.5065 ^a	215.0268 ^a
$\langle \delta(\mathbf{r}_i) \rangle$	72.517(30) ^b	129.490(30) ^b	210.715(40) ^b
	71.9(2) ^d	128.5(5) ^d	211(1) ^d
	O V	F VI	Ne VII
K_{NMS}	68.3908 ^a	88.0730 ^a	110.2547 ^a
$\langle -\frac{1}{2}\nabla_i^2 \rangle$	68.41085 ^b	88.10012 ^b	110.2881 ^b
K_{SMS}	0.9143 ^a	0.9913 ^a	1.0549 ^a
$-\langle \nabla_i \cdot \nabla_j \rangle$	0.90194(50) ^b	0.97224(50) ^b	1.0247(40) ^b
	0.902377 ^c	0.972739 ^c	1.027164 ^c
$\rho^e(\mathbf{0})$	328.7705 ^a	477.9292 ^a	667.9708 ^a
$\langle \delta(\mathbf{r}_i) \rangle$	320.212(40) ^b	462.46(40) ^b	642.10(50) ^b
	318(1) ^d	460(1) ^d	639(3) ^d

^a This work ^b King *et al.* [49]
^c Komasa *et al.* [50] ^d Galvez *et al.* [51]

Table 6

Wavenumber mass shift $\delta\sigma_{\text{MS}}$ and field shift $\delta\sigma_{\text{FS}}$ (in cm^{-1}) for the $1s^2 2s 2p \ ^3P_1^o - \ ^3P_2^o$ in Ar^{14+} for the isotope pair $^{40,36}\text{Ar}$.

		$\delta\sigma_{\text{MS}}^{40,36}$	$\delta\sigma_{\text{FS}}^{40,36}$
Theory	this work	0.0359	-0.00012
	Orts <i>et al.</i> [52]	0.0359	-0.0001
Observation	Orts <i>et al.</i> [52]	0.0340(28)	

Table 7

Total energies (in E_h), excitation energies (in cm^{-1}), normal and specific mass shift \tilde{K} parameters (in GHz u), \tilde{F} field shift factors (in GHz/fm²) for levels in the boron isoelectronic sequence ($8 \leq Z \leq 30$ and $Z = 36, 42$). For each of the many-electron wave functions, the leading components are given in the *LSJ* coupling scheme. The number in square brackets is the power of 10. See page 17 for Explanation of Tables.

Level composition in <i>LSJ</i> coupling				J	Energy (E_h)	ΔE (cm^{-1})	\tilde{K}_{NMS} (GHz u)	\tilde{K}_{SMS} (GHz u)	\tilde{F} (GHz/fm ²)
O IV									
$1s^2 2s^2 2p^2 2P^o$	(95%) + $1s^2 2p^3 2P^o$	(4%)	1/2	-71.3006468	0.00	2.5709821[5]	-3.8411303[3]	1.283334[1]	
	(95%) + $1s^2 2p^3 2P^o$	(4%)	3/2	-71.2988722	389.49	2.5709779[5]	-3.8498436[3]	1.283339[1]	
$1s^2 2s 2p^2 4P$	(100%)		1/2	-70.9755351	71353.76	2.5592579[5]	-1.1295016[4]	1.243923[1]	
	(100%)		3/2	-70.9749349	71485.49	2.5592561[5]	-1.1298419[4]	1.243924[1]	
	(100%)		5/2	-70.9740914	71670.63	2.5592683[5]	-1.1305008[4]	1.243926[1]	
$1s^2 2s 2p^2 2D$	(98%) + $1s^2 2s^2 3d 2D$	(1%)	5/2	-70.7218546	127030.20	2.5504401[5]	-1.0975396[4]	1.242509[1]	
	(98%) + $1s^2 2s^2 3d 2D$	(1%)	3/2	-70.7217904	127044.30	2.5504327[5]	-1.0973347[4]	1.242510[1]	
$1s^2 2s 2p^2 2S$	(99%)		1/2	-70.5504716	164644.42	2.5444548[5]	-9.6766354[3]	1.242576[1]	
$1s^2 2s 2p^2 2P$	(98%) + $1s^2 2p^2 3d 2P$	(1%)	1/2	-70.4776245	180632.51	2.5417421[5]	-9.9012304[3]	1.237490[1]	
	(98%) + $1s^2 2p^2 3d 2P$	(1%)	3/2	-70.4765123	180876.62	2.5417477[5]	-9.9072673[3]	1.237491[1]	
$1s^2 2p^3 4S^o$	(99%)		3/2	-70.2459347	231482.54	2.5330250[5]	-1.7439323[4]	1.197574[1]	
$1s^2 2p^3 2D^o$	(97%) + $1s^2 2s 2p 3d 2D^o$	(2%)	5/2	-70.1376733	255243.17	2.5293819[5]	-1.8154350[4]	1.199250[1]	
	(97%) + $1s^2 2s 2p 3d 2D^o$	(2%)	3/2	-70.1375436	255271.63	2.5293646[5]	-1.8152910[4]	1.199253[1]	
$1s^2 2p^3 2P^o$	(94%) + $1s^2 2s^2 2p 2P^o$	(4%)	1/2	-69.9825047	289298.75	2.5240503[5]	-1.6483349[4]	1.201038[1]	
	(94%) + $1s^2 2s^2 2p 2P^o$	(4%)	3/2	-69.9824759	289305.06	2.5240548[5]	-1.6484940[4]	1.201044[1]	
F V									
$1s^2 2s^2 2p^2 2P^o$	(96%) + $1s^2 2p^3 2P^o$	(4%)	1/2	-92.3744980	0.00	3.3302241[5]	-6.6294003[3]	2.100154[1]	
	(96%) + $1s^2 2p^3 2P^o$	(4%)	3/2	-92.3710819	749.75	3.3301970[5]	-6.6452870[3]	2.100154[1]	
$1s^2 2s 2p^2 4P$	(100%)		1/2	-91.9840119	85701.79	3.3161481[5]	-1.7127851[4]	2.030332[1]	
	(100%)		3/2	-91.9828551	85955.69	3.3161392[5]	-1.7133606[4]	2.030332[1]	
	(100%)		5/2	-91.9811967	86319.66	3.3161501[5]	-1.7144459[4]	2.030334[1]	
$1s^2 2s 2p^2 2D$	(99%)		5/2	-91.6775124	152970.67	3.3054283[5]	-1.6797728[4]	2.027780[1]	
	(99%)		3/2	-91.6774085	152993.48	3.3054168[5]	-1.6794403[4]	2.027781[1]	
$1s^2 2s 2p^2 2S$	(99%)		1/2	-91.4731655	197819.62	3.2982345[5]	-1.5255295[4]	2.027840[1]	
$1s^2 2s 2p^2 2P$	(98%) + $1s^2 2p^2 3d 2P$	(1%)	1/2	-91.3947240	215035.55	3.2953097[5]	-1.5755447[4]	2.019876[1]	
	(98%) + $1s^2 2p^2 3d 2P$	(1%)	3/2	-91.3925896	215503.99	3.2953080[5]	-1.5765881[4]	2.019874[1]	
$1s^2 2p^3 4S^o$	(100%)		3/2	-91.1152847	276365.39	3.2849107[5]	-2.6342623[4]	1.949263[1]	
$1s^2 2p^3 2D^o$	(98%) + $1s^2 2s 2p 3d 2D^o$	(1%)	5/2	-90.9742390	307321.32	3.2800832[5]	-2.7035295[4]	1.951334[1]	
	(98%) + $1s^2 2s 2p 3d 2D^o$	(1%)	3/2	-90.9740253	307368.24	3.2800535[5]	-2.7032454[4]	1.951338[1]	
$1s^2 2p^3 2P^o$	(95%) + $1s^2 2s^2 2p 2P^o$	(3%)	1/2	-90.7904091	347667.33	3.2736681[5]	-2.4959091[4]	1.954643[1]	
	(95%) + $1s^2 2s^2 2p 2P^o$	(3%)	3/2	-90.7903223	347686.38	3.2736773[5]	-2.4960417[4]	1.954659[1]	
Ne VI									
$1s^2 2s^2 2p^2 2P^o$	(96%) + $1s^2 2p^3 2P^o$	(3%)	1/2	-116.2144066	0.00	4.1887574[5]	-1.0000115[4]	3.263471[1]	
	(96%) + $1s^2 2p^3 2P^o$	(3%)	3/2	-116.2084301	1311.69	4.1886813[5]	-1.0026618[4]	3.263449[1]	
$1s^2 2s 2p^2 4P$	(100%)		1/2	-115.7578445	100203.78	4.1722827[5]	-2.4075677[4]	3.148280[1]	
	(100%)		3/2	-115.7558093	100650.45	4.1722599[5]	-2.4084806[4]	3.148278[1]	
	(100%)		5/2	-115.7528583	101298.12	4.1722621[5]	-2.4101636[4]	3.148278[1]	
$1s^2 2s 2p^2 2D$	(99%)		5/2	-115.3983960	179093.62	4.1596816[5]	-2.3741328[4]	3.144186[1]	
	(99%)		3/2	-115.3982489	179125.89	4.1596643[5]	-2.3736237[4]	3.144187[1]	
$1s^2 2s 2p^2 2S$	(99%)		1/2	-115.1614234	231103.08	4.1512942[5]	-2.1951027[4]	3.144235[1]	
$1s^2 2s 2p^2 2P$	(99%)		1/2	-115.0778033	249455.56	4.1481785[5]	-2.2729332[4]	3.132526[1]	
	(99%)		3/2	-115.0740873	250271.13	4.1481576[5]	-2.2746262[4]	3.132507[1]	
$1s^2 2p^3 4S^o$	(100%)		3/2	-114.7492420	321566.45	4.1360337[5]	-3.6937191[4]	3.015898[1]	
$1s^2 2p^3 2D^o$	(99%) + $1s^2 2s 2p 3d 2D^o$	(1%)	5/2	-114.5757414	359645.42	4.1300391[5]	-3.7607547[4]	3.018435[1]	
	(99%) + $1s^2 2s 2p 3d 2D^o$	(1%)	3/2	-114.5754351	359712.64	4.1299922[5]	-3.7602259[4]	3.018444[1]	
$1s^2 2p^3 2P^o$	(95%) + $1s^2 2s^2 2p 2P^o$	(3%)	1/2	-114.3633952	406250.02	4.1225682[5]	-3.5100735[4]	3.024024[1]	
	(95%) + $1s^2 2s^2 2p 2P^o$	(3%)	3/2	-114.3631900	406295.06	4.1225833[5]	-3.5101518[4]	3.024062[1]	
Na VII									
$1s^2 2s^2 2p^2 2P^o$	(96%) + $1s^2 2p^3 2P^o$	(3%)	1/2	-142.8237703	0.00	5.1465585[5]	-1.3948097[4]	4.863338[1]	
	(96%) + $1s^2 2p^3 2P^o$	(3%)	3/2	-142.8140130	2141.49	5.1464141[5]	-1.3990526[4]	4.863263[1]	
$1s^2 2s 2p^2 4P$	(100%)		1/2	-142.3001524	114920.84	5.1276506[5]	-3.2133335[4]	4.683444[1]	
	(100%)		3/2	-142.2968073	115655.00	5.1276044[5]	-3.2147166[4]	4.683436[1]	
	(100%)		5/2	-142.2919322	116724.97	5.1275856[5]	-3.2172029[4]	4.683428[1]	
$1s^2 2s 2p^2 2D$	(99%)		5/2	-141.8873335	205524.11	5.1131581[5]	-3.1799477[4]	4.677339[1]	
	(99%)		3/2	-141.8871517	205564.02	5.1131339[5]	-3.1791977[4]	4.677340[1]	
$1s^2 2s 2p^2 2S$	(99%)		1/2	-141.6179937	264637.36	5.1035818[5]	-2.9759949[4]	4.677351[1]	
$1s^2 2s 2p^2 2P$	(99%)		1/2	-141.5295801	284041.90	5.1002936[5]	-3.0814334[4]	4.660942[1]	
	(99%)		3/2	-141.5235794	285358.92	5.1002365[5]	-3.0841088[4]	4.660871[1]	
$1s^2 2p^3 4S^o$	(100%)		3/2	-141.1503494	367273.41	5.0863559[5]	-4.9210618[4]	4.478441[1]	
$1s^2 2p^3 2D^o$	(99%) + $1s^2 2s 2p 3d 2D^o$	(1%)	5/2	-140.9445975	412430.74	5.0792099[5]	-4.9860181[4]	4.481509[1]	
	(99%) + $1s^2 2s 2p 3d 2D^o$	(1%)	3/2	-140.9442158	412514.53	5.0791402[5]	-4.9850673[4]	4.481529[1]	
$1s^2 2p^3 2P^o$	(96%) + $1s^2 2s^2 2p 2P^o$	(3%)	1/2	-140.7038601	465266.50	5.0706893[5]	-4.6897702[4]	4.490355[1]	

Continued...

Table 8

Upper part: individual contributions to the wavenumber mass shift $\delta\sigma_{\text{MS}}$ of the forbidden transition $1s^2 2s^2 2p \ ^2P_{1/2}^o - \ ^2P_{3/2}^o$ in boron-like $^{36,40}\text{Ar}^{13+}$. Lower part: wavenumber mass, field and total shifts. All numbers in cm^{-1} .

		$\delta\sigma_{\text{MS}}$			
		$\langle H_{\text{NMS}}^1 \rangle$	$\langle H_{\text{NMS}}^2 + H_{\text{NMS}}^3 \rangle$	$\langle H_{\text{SMS}}^1 \rangle$	$\langle H_{\text{SMS}}^2 + H_{\text{SMS}}^3 \rangle$
Theory	This work	0.1054	-0.0821	-0.0745	0.1150
	Tupitsyn <i>et al.</i> [16]	0.1053	-0.0822	-0.0742	0.1151
		$\delta\sigma_{\text{MS}}$	$\delta\sigma_{\text{FS}}$	$\delta\sigma$	
Theory	This work	0.0639	-0.00053	0.0633	
	Tupitsyn <i>et al.</i> [16]	0.0640			
	Orts <i>et al.</i> [52]	0.0640 ^a	-0.0005	0.0635	
Observed	Orts <i>et al.</i> [52]			0.0640(31)	

^a the QED contributions (-0.0006 cm^{-1}) have been subtracted from their estimation for a fair comparison.

Table 9

Comparison of MCHF and MCDHF specific mass shift parameters for O IV (in atomic units $E_h m_e$).

	MCHF	MCDHF		
		J	K_{SMS}^1	K_{SMS}
$2s^2 2p \ ^2P^o$	-1.07928	1/2	-1.0703	-1.0642
		3/2	-1.0654	-1.0666
$2s 2p^2 \ ^4P$	-3.14595	1/2	-3.1404	-3.1293
		3/2	-3.1388	-3.1302
		5/2	-3.1365	-3.1320
$2s 2p^2 \ ^2D$	-3.05072	5/2	-3.0476	-3.0407
		3/2	-3.0472	-3.0401
$2s 2p^2 \ ^2P$	-2.75703	1/2	-2.7544	-2.7431
		3/2	-2.7511	-2.7448
$2s 2p^2 \ ^2S$	-2.6815	1/2	-2.6877	-2.6809
$2p^3 \ ^4S^o$	-4.8515	3/2	-4.8454	-4.8315
$2p^3 \ ^2D^o$	-5.0423	5/2	-5.0427	-5.0296
		3/2	-5.0425	-5.0292
$2p^3 \ ^2P^o$	-4.5694	1/2	-4.5796	-4.5667
		3/2	-4.5794	-4.5671

Table 10 (continued)

Level composition in LSJ coupling			J	Energy (E_h)	ΔE (cm^{-1})	\tilde{K}_{NMS} (GHz u)	\tilde{K}_{SMS} (GHz u)	\tilde{F} (GHz/fm ²)
$1s^2 2s 2p^3 \ ^3P^o$	(99%)		2	-120.0520265	175976.73	4.3273359[5]	-3.3336407[4]	3.130776[1]
	(99%)		1	-120.0519193	176000.26	4.3273247[5]	-3.3335732[4]	3.130783[1]
	(99%)		2	-119.9045366	208347.03	4.3222021[5]	-3.2360725[4]	3.130919[1]
	(99%)		1	-119.9045144	208351.89	4.3221917[5]	-3.2355672[4]	3.130923[1]
	(99%)		0	-119.9043467	208388.69	4.3221711[5]	-3.2353726[4]	3.130922[1]
	(98%)	+ $1s^2 2p^3 3d \ ^1D^o$ (1%)	2	-119.6197268	270855.55	4.3121873[5]	-3.2200343[4]	3.121746[1]
	(98%)	+ $1s^2 2p^3 3d \ ^3S^o$ (1%)	1	-119.5799645	279582.37	4.3106150[5]	-3.1141988[4]	3.114991[1]
	(98%)	+ $1s^2 2p^3 3d \ ^1P^o$ (1%)	1	-119.4673898	304289.64	4.3069420[5]	-3.0770978[4]	3.121536[1]
	(96%)	+ $1s^2 2s^2 2p^2 \ ^3P$ (1%)	2	-118.9724357	412919.52	4.2887332[5]	-4.3791251[4]	3.015218[1]
	(96%)	+ $1s^2 2s^2 2p^2 \ ^3P$ (1%)	1	-118.9688252	413711.94	4.2886747[5]	-4.3806971[4]	3.015194[1]
	(96%)	+ $1s^2 2s^2 2p^2 \ ^3P$ (1%)	0	-118.9672331	414061.36	4.2886704[5]	-4.3813926[4]	3.015185[1]
$1s^2 2p^4 \ ^1D$	+ $1s^2 2s^2 2p^2 3d \ ^1D$ (2%)	2	-118.8629831	436941.59	4.2850606[5]	-4.4366859[4]	3.016815[1]	
$1s^2 2p^4 \ ^1S$	+ $1s^2 2s^2 2p^2 \ ^1S$ (5%)	0	-118.5702476	501189.59	4.2751002[5]	-4.1271948[4]	3.022496[1]	
Na VI								
$1s^2 2s^2 2p^2 \ ^3P$	(98%)	+ $1s^2 2p^4 \ ^3P$ (1%)	0	-149.1523282	0.00	5.3747474[5]	-2.8518535[4]	4.831292[1]
	(98%)	+ $1s^2 2p^4 \ ^3P$ (1%)	1	-149.1491632	694.64	5.3747016[5]	-2.8532374[4]	4.831285[1]
$1s^2 2s^2 2p^2 \ ^1D$	(98%)	+ $1s^2 2p^4 \ ^3P$ (1%)	2	-149.1438748	1855.29	5.3746734[5]	-2.8560428[4]	4.831259[1]
	(98%)	+ $1s^2 2p^4 \ ^1D$ (1%)	2	-148.9899158	35645.39	5.3692690[5]	-2.8333272[4]	4.832039[1]
$1s^2 2s^2 2p^2 \ ^1S$	+ $1s^2 2p^4 \ ^1S$ (5%)	0	-148.8122141	74646.40	5.3630426[5]	-2.8431579[4]	4.823194[1]	
$1s^2 2s 2p^3 \ ^5S^o$	(100%)		2	-148.6839554	102795.94	5.3577143[5]	-4.5438128[4]	4.662505[1]
$1s^2 2s 2p^3 \ ^3D^o$	(99%)		3	-148.2218363	204219.37	5.3414460[5]	-4.4958576[4]	4.657718[1]
	(99%)		2	-148.2214102	204312.88	5.3413821[5]	-4.4949541[4]	4.657722[1]
$1s^2 2s 2p^3 \ ^3P^o$	(99%)		1	-148.2212300	204352.43	5.3413651[5]	-4.4947516[4]	4.657732[1]
	(99%)		2	-148.0518783	241520.82	5.3354163[5]	-4.3808299[4]	4.657872[1]
$1s^2 2s 2p^3 \ ^3P^o$	(99%)		1	-148.0518733	241521.92	5.3354005[5]	-4.3801210[4]	4.657879[1]
	(99%)		0	-148.0516551	241569.81	5.3353701[5]	-4.3797835[4]	4.657876[1]
$1s^2 2s 2p^3 \ ^1D^o$	+ $1s^2 2s^2 2p 3d \ ^1D^o$ (1%)	2	-147.7278257	312642.15	5.3239840[5]	-4.3796254[4]	4.644381[1]	
$1s^2 2s 2p^3 \ ^3S^o$	+ $1s^2 2p^3 3d \ ^3S^o$ (1%)	1	-147.6906078	320810.53	5.3224966[5]	-4.2783235[4]	4.635106[1]	
$1s^2 2s 2p^3 \ ^1P^o$	(98%)		1	-147.5540602	350779.26	5.3178916[5]	-4.2214680[4]	4.644162[1]
$1s^2 2p^4 \ ^3P$	(97%)	+ $1s^2 2s^2 2p^2 \ ^3P$ (1%)	2	-146.9767101	477492.96	5.2968187[5]	-5.9033810[4]	4.476218[1]
	(97%)	+ $1s^2 2s^2 2p^2 \ ^3P$ (1%)	1	-146.9706997	478812.10	5.2967086[5]	-5.9058214[4]	4.476156[1]
$1s^2 2p^4 \ ^3P$	(97%)	+ $1s^2 2s^2 2p^2 \ ^3P$ (1%)	0	-146.9680970	479383.31	5.2966855[5]	-5.9068985[4]	4.476132[1]
	(96%)	+ $1s^2 2s^2 2p^2 \ ^1D$ (1%)	2	-146.8446022	506487.29	5.2923567[5]	-5.9606664[4]	4.478194[1]
$1s^2 2p^4 \ ^1S$	+ $1s^2 2s^2 2p^2 \ ^1S$ (5%)	0	-146.5103524	579846.65	5.2808449[5]	-5.5918343[4]	4.487240[1]	
Mg VII								
$1s^2 2s^2 2p^2 \ ^3P$	(98%)	+ $1s^2 2p^4 \ ^3P$ (1%)	0	-180.4759625	0.00	6.5017426[5]	-3.7302034[4]	6.961339[1]
	(98%)	+ $1s^2 2p^4 \ ^3P$ (1%)	1	-180.4708952	1112.14	6.5016618[5]	-3.7323672[4]	6.961315[1]
$1s^2 2s^2 2p^2 \ ^1D$	(98%)	+ $1s^2 2p^4 \ ^3P$ (1%)	2	-180.4626198	2928.38	6.5015867[5]	-3.7365019[4]	6.961240[1]
	(98%)	+ $1s^2 2p^4 \ ^1D$ (1%)	2	-180.2887088	41097.43	6.4954376[5]	-3.7118340[4]	6.962177[1]
$1s^2 2s^2 2p^2 \ ^1S$	+ $1s^2 2p^4 \ ^1S$ (5%)	0	-180.0869194	85385.08	6.4883236[5]	-3.7304762[4]	6.948665[1]	
$1s^2 2s 2p^3 \ ^5S^o$	(100%)		2	-179.9387744	117899.16	6.4822713[5]	-5.8741789[4]	6.706538[1]
$1s^2 2s 2p^3 \ ^3D^o$	(99%)		3	-179.4145625	232950.36	6.4638052[5]	-5.8244593[4]	6.699491[1]
	(99%)		2	-179.4140639	233059.80	6.4637160[5]	-5.8230040[4]	6.699496[1]
$1s^2 2s 2p^3 \ ^3P^o$	(99%)		1	-179.4137787	233122.38	6.4636918[5]	-5.8226539[4]	6.699512[1]
	(99%)		1	-179.2224979	275103.67	6.4569609[5]	-5.6917275[4]	6.699663[1]
$1s^2 2s 2p^3 \ ^3P^o$	(99%)		2	-179.2224402	275116.33	6.4569832[5]	-5.6927461[4]	6.699652[1]
	(99%)		0	-179.2222352	275161.32	6.4569190[5]	-5.6911788[4]	6.699660[1]
$1s^2 2s 2p^3 \ ^1D^o$	(99%)		2	-178.8596168	354746.86	6.4441436[5]	-5.7071082[4]	6.680792[1]
$1s^2 2s 2p^3 \ ^3S^o$	+ $1s^2 2p^3 3d \ ^3S^o$ (1%)	1	-178.8248988	362366.58	6.4427417[5]	-5.6095580[4]	6.668425[1]	
$1s^2 2s 2p^3 \ ^1P^o$	(99%)		1	-178.6426646	397621.71	6.4372809[5]	-5.5334394[4]	6.680549[1]
$1s^2 2p^4 \ ^3P$	(97%)	+ $1s^2 2s^2 2p^2 \ ^3P$ (1%)	2	-178.0038944	542556.21	6.4131677[5]	-7.6506015[4]	6.426951[1]
	(97%)	+ $1s^2 2s^2 2p^2 \ ^3P$ (1%)	1	-177.9944361	544632.08	6.4129782[5]	-7.6542489[4]	6.426810[1]
$1s^2 2p^4 \ ^3P$	(97%)	+ $1s^2 2s^2 2p^2 \ ^3P$ (1%)	0	-177.9904328	545510.69	6.4129255[5]	-7.6557577[4]	6.426758[1]
	(97%)	+ $1s^2 2s^2 2p^2 \ ^1D$ (1%)	2	-177.8485246	576655.93	6.4079062[5]	-7.7076061[4]	6.429317[1]
$1s^2 2p^4 \ ^1S$	+ $1s^2 2s^2 2p^2 \ ^1S$ (5%)	0	-177.4729958	659074.98	6.3948810[5]	-7.2775612[4]	6.443054[1]	
Al VIII								
$1s^2 2s^2 2p^2 \ ^3P$	(98%)	+ $1s^2 2p^4 \ ^3P$ (1%)	0	-214.8293779	0.00	7.7370703[5]	-4.7193228[4]	9.748364[1]
	(98%)	+ $1s^2 2p^4 \ ^3P$ (1%)	1	-214.8215927	1708.66	7.7369357[5]	-4.7225811[4]	9.748310[1]
$1s^2 2s^2 2p^2 \ ^1D$	(98%)	+ $1s^2 2p^4 \ ^3P$ (1%)	2	-214.8092653	4414.19	7.7367877[5]	-4.7284375[4]	9.748140[1]
	(98%)	+ $1s^2 2p^4 \ ^1D$ (1%)	2	-214.6158188	46870.79	7.7299163[5]	-4.7018717[4]	9.749258[1]
$1s^2 2s^2 2p^2 \ ^1S$	+ $1s^2 2p^4 \ ^1S$ (5%)	0	-214.3898451	96466.29	7.7219188[5]	-4.7318221[4]	9.729482[1]	
$1s^2 2s 2p^3 \ ^5S^o$	(100%)		2	-214.2205307	133626.50	7.7150665[5]	-7.3703660[4]	9.377590[1]
$1s^2 2s 2p^3 \ ^3D^o$	(99%)		3	-213.6344142	262264.20	7.6944239[5]	-7.3192294[4]	9.367712[1]
	(99%)		2	-213.6339348	262369.42	7.6943041[5]	-7.3169529[4]	9.367723[1]
$1s^2 2s 2p^3 \ ^3P^o$	(99%)		1	-213.6335011	262464.60	7.6942705[5]	-7.3164573[4]	9.367743[1]
	(99%)		1	-213.4202377	309270.52	7.6867772[5]	-7.1694525[4]	9.367895[1]
$1s^2 2s 2p^3 \ ^3P^o$	(99%)		2	-213.4200302	309316.05	7.6868072[5]	-7.1709425[4]	9.367878[1]
	(99%)		0	-213.4199551	309332.54	7.6867213[5]	-7.1685833[4]	9.367895[1]

Continued ...

Table 10 (continued)

Level composition in LSJ coupling				J	Energy (E_{h})	ΔE (cm $^{-1}$)	\tilde{K}_{NMS} (GHz u)	\tilde{K}_{SMS} (GHz u)	\tilde{F} (GHz/fm 2)
$1s^2 2s 2p^3 \ ^1D^{\circ}$	(99%)			2	-213.0187642	397383.75	7.6725826[5]	-7.2012426[4]	9.342435[1]
$1s^2 2s 2p^3 \ ^3S^{\circ}$	(99%)			1	-212.9866294	404436.54	7.6712586[5]	-7.1067630[4]	9.326336[1]
$1s^2 2s 2p^3 \ ^1P^{\circ}$	(99%)			1	-212.8016794	445028.35	7.6649471[5]	-7.0118011[4]	9.342148[1]
$1s^2 2p^4 \ ^3P$	(97%)	$+ 1s^2 2s^2 2p^2 \ ^3P$	(1%)	2	-212.0576804	608317.26	7.6377550[5]	-9.6193453[4]	8.973057[1]
	(98%)	$+ 1s^2 2s^2 2p^2 \ ^3P$	(1%)	1	-212.0434414	611442.35	7.6374511[5]	-9.6246585[4]	8.972768[1]
	(98%)	$+ 1s^2 2s^2 2p^2 \ ^3P$	(1%)	0	-212.0375899	612726.61	7.6373544[5]	-9.6265975[4]	8.972674[1]
$1s^2 2p^4 \ ^1D$	(97%)	$+ 1s^2 2s^2 2p^2 \ ^1D$	(1%)	2	-211.8782649	647694.41	7.6316824[5]	-9.6763178[4]	8.975809[1]
$1s^2 2p^4 \ ^1S$	(94%)	$+ 1s^2 2s^2 2p^2 \ ^1S$	(5%)	0	-211.4615836	739145.38	7.6171636[5]	-9.1830163[4]	8.995855[1]
Si IX									
$1s^2 2s^2 2p^2 \ ^3P$	(98%)	$+ 1s^2 2p^4 \ ^3P$	(1%)	0	-252.2179198	0.00	9.0807449[5]	-5.8184611[4]	1.332544[2]
	(98%)	$+ 1s^2 2p^4 \ ^3P$	(1%)	1	-252.2063456	2540.25	9.0805315[5]	-5.8232155[4]	1.332533[2]
	(98%)	$+ 1s^2 2p^4 \ ^3P$	(1%)	2	-252.1887113	6410.52	9.0802778[5]	-5.8312314[4]	1.332500[2]
$1s^2 2s^2 2p^2 \ ^1D$	(98%)	$+ 1s^2 2p^4 \ ^1D$	(1%)	2	-251.9761136	53070.34	9.0727130[5]	-5.8029075[4]	1.332632[2]
$1s^2 2s^2 2p^2 \ ^1S$	(95%)	$+ 1s^2 2p^4 \ ^1S$	(5%)	0	-251.7257592	108016.77	9.0638424[5]	-5.8465591[4]	1.329837[2]
$1s^2 2s 2p^3 \ ^5S^{\circ}$	(100%)			2	-251.5339219	150120.18	9.0561080[5]	-9.0316805[4]	1.280200[2]
$1s^2 2s 2p^3 \ ^3D^{\circ}$	(99%)			3	-250.8859967	292323.33	9.0332982[5]	-8.9794054[4]	1.278865[2]
	(99%)	$+ 1s^2 2s 2p^3 \ ^3P^{\circ}$	(1%)	2	-250.8857182	292384.45	9.0331441[5]	-8.9759179[4]	1.278867[2]
	(99%)			1	-250.8850767	292525.24	9.0330983[5]	-8.9752975[4]	1.278870[2]
$1s^2 2s 2p^3 \ ^3P^{\circ}$	(99%)			1	-250.6496224	344201.49	9.0248383[5]	-8.8125643[4]	1.278884[2]
	(100%)			0	-250.6493735	344256.11	9.0247665[5]	-8.8112042[4]	1.278885[2]
	(99%)	$+ 1s^2 2s 2p^3 \ ^3D^{\circ}$	(1%)	2	-250.6091157	344312.68	9.0248762[5]	-8.8147636[4]	1.278881[2]
$1s^2 2s 2p^3 \ ^1D^{\circ}$	(99%)			2	-250.2097125	440750.55	9.0092836[5]	-8.8610292[4]	1.275543[2]
$1s^2 2s 2p^3 \ ^3S^{\circ}$	(99%)	$+ 1s^2 2s 2p^3 \ ^1P^{\circ}$	(1%)	1	-250.1803542	447193.95	9.0080351[5]	-8.7689509[4]	1.273490[2]
$1s^2 2s 2p^3 \ ^1P^{\circ}$	(99%)	$+ 1s^2 2s 2p^3 \ ^3S^{\circ}$	(1%)	1	-249.9706514	493218.39	9.0008656[5]	-8.6557980[4]	1.275506[2]
$1s^2 2p^4 \ ^3P$	(97%)	$+ 1s^2 2s^2 2p^2 \ ^3P$	(1%)	2	-249.1424537	674986.77	8.9705607[5]	-1.1808314[5]	1.223398[2]
	(98%)	$+ 1s^2 2s^2 2p^2 \ ^3P$	(1%)	1	-249.1217695	679526.43	8.9700965[5]	-1.1815892[5]	1.223342[2]
	(98%)	$+ 1s^2 2s^2 2p^2 \ ^3P$	(1%)	0	-249.1135840	681322.94	8.9699392[5]	-1.1818160[5]	1.223327[2]
$1s^2 2p^4 \ ^1D$	(97%)	$+ 1s^2 2s^2 2p^2 \ ^1D$	(1%)	2	-248.9379625	719867.40	8.9636547[5]	-1.1865703[5]	1.223708[2]
$1s^2 2p^4 \ ^1S$	(94%)	$+ 1s^2 2s^2 2p^2 \ ^1S$	(5%)	0	-248.4801742	820340.32	8.9476528[5]	-1.1307182[5]	1.226538[2]
P X									
$1s^2 2s^2 2p^2 \ ^3P$	(98%)	$+ 1s^2 2p^4 \ ^3P$	(1%)	0	-292.6475879	0.00	1.0532773[6]	-7.0267104[4]	1.784203[2]
	(98%)	$+ 1s^2 2p^4 \ ^3P$	(1%)	1	-292.6308367	3676.45	1.0532447[6]	-7.0334576[4]	1.784184[2]
	(98%)	$+ 1s^2 2p^4 \ ^3P$	(1%)	2	-292.6064592	9026.70	1.0532048[6]	-7.0440977[4]	1.784124[2]
$1s^2 2s^2 2p^2 \ ^1D$	(98%)	$+ 1s^2 2p^4 \ ^1D$	(1%)	2	-292.3750067	59824.65	1.0523859[6]	-7.0144346[4]	1.784278[2]
$1s^2 2s^2 2p^2 \ ^1S$	(94%)	$+ 1s^2 2p^4 \ ^1S$	(5%)	0	-292.0999630	120189.76	1.0514182[6]	-7.0742022[4]	1.780442[2]
$1s^2 2s 2p^3 \ ^5S^{\circ}$	(100%)			2	-291.8842161	167540.74	1.0505400[6]	-1.0857385[5]	1.712162[2]
$1s^2 2s 2p^3 \ ^3D^{\circ}$	(99%)	$+ 1s^2 2s 2p^3 \ ^3P^{\circ}$	(1%)	2	-291.1747264	323255.71	1.0480238[6]	-1.0798983[5]	1.710411[2]
	(100%)			3	-291.1744907	323307.44	1.0480430[6]	-1.0804235[5]	1.710407[2]
	(99%)			1	-291.1737983	323459.40	1.0480177[6]	-1.0798285[5]	1.710414[2]
$1s^2 2s 2p^3 \ ^3P^{\circ}$	(99%)			1	-290.9157546	380093.46	1.0471143[6]	-1.0620383[5]	1.710424[2]
	(100%)			0	-290.9156356	380119.59	1.0471053[6]	-1.0618278[5]	1.710428[2]
	(99%)	$+ 1s^2 2s 2p^3 \ ^3D^{\circ}$	(1%)	2	-290.9147096	380322.81	1.0471188[6]	-1.0623633[5]	1.710419[2]
$1s^2 2s 2p^3 \ ^1D^{\circ}$	(99%)			2	-290.4375065	485056.78	1.0454241[6]	-1.0685572[5]	1.706137[2]
$1s^2 2s 2p^3 \ ^3S^{\circ}$	(98%)	$+ 1s^2 2s 2p^3 \ ^1P^{\circ}$	(1%)	1	-290.4112655	490816.02	1.0453069[6]	-1.0595151[5]	1.703566[2]
$1s^2 2s 2p^3 \ ^1P^{\circ}$	(98%)	$+ 1s^2 2s 2p^3 \ ^3S^{\circ}$	(1%)	1	-290.1760976	542429.39	1.0445029[6]	-1.0464772[5]	1.706084[2]
$1s^2 2p^4 \ ^3P$	(97%)	$+ 1s^2 2s^2 2p^2 \ ^3P$	(1%)	2	-289.2632122	742784.59	1.0411583[6]	-1.42116291[5]	1.634375[2]
	(98%)	$+ 1s^2 2s^2 2p^2 \ ^3P$	(1%)	1	-289.2340348	749188.29	1.0410903[6]	-1.4226902[5]	1.634276[2]
	(98%)	$+ 1s^2 2s^2 2p^2 \ ^3P$	(1%)	0	-289.2230240	751604.88	1.0410665[6]	-1.4229228[5]	1.634254[2]
$1s^2 2p^4 \ ^1D$	(97%)	$+ 1s^2 2s^2 2p^2 \ ^1D$	(1%)	2	-289.0323005	793463.84	1.0403814[6]	-1.4274750[5]	1.634712[2]
$1s^2 2p^4 \ ^1S$	(94%)	$+ 1s^2 2s^2 2p^2 \ ^1S$	(5%)	0	-288.5333498	902970.85	1.0386350[6]	-1.3649334[5]	1.638598[2]
S XI									
$1s^2 2s^2 2p^2 \ ^3P$	(98%)	$+ 1s^2 2p^4 \ ^3P$	(1%)	0	-336.1250101	0.00	1.2093283[6]	-8.3443437[4]	2.346528[2]
	(98%)	$+ 1s^2 2p^4 \ ^3P$	(1%)	1	-336.1013056	5202.55	1.2092805[6]	-8.3537074[4]	2.346499[2]
	(97%)	$+ 1s^2 2p^4 \ ^3P$	(1%)	2	-336.0685879	12383.25	1.2092215[6]	-8.3674249[4]	2.346398[2]
$1s^2 2s^2 2p^2 \ ^1D$	(97%)	$+ 1s^2 2p^4 \ ^1D$	(1%)	2	-335.8184121	67290.49	1.2083221[6]	-8.3361299[4]	2.346576[2]
$1s^2 2s^2 2p^2 \ ^1S$	(94%)	$+ 1s^2 2p^4 \ ^1S$	(5%)	0	-335.5183558	133145.23	1.2072417[6]	-8.4126914[4]	2.341448[2]
$1s^2 2s 2p^3 \ ^5S^{\circ}$	(100%)			2	-335.2772346	186065.22	1.2062947[6]	-1.2846679[5]	2.249504[2]
$1s^2 2s 2p^3 \ ^3D^{\circ}$	(98%)	$+ 1s^2 2s 2p^3 \ ^3P^{\circ}$	(1%)	2	-334.5068680	355141.13	1.2035596[6]	-1.2785165[5]	2.247258[2]
	(100%)			3	-334.5056214	355414.74	1.2035825[6]	-1.2792948[5]	2.247248[2]
	(99%)	$+ 1s^2 2s 2p^3 \ ^3P^{\circ}$	(1%)	1	-334.5055518	355430.00	1.2035516[6]	-1.2784468[5]	2.247259[2]
$1s^2 2s 2p^3 \ ^3P^{\circ}$	(100%)			0	-334.2244366	417127.67	1.2025589[6]	-1.2589036[5]	2.247272[2]
	(99%)	$+ 1s^2 2s 2p^3 \ ^3D^{\circ}$	(1%)	1	-334.2242702	417164.19	1.2025698[6]	-1.2592252[5]	2.247260[2]
	(98%)	$+ 1s^2 2s 2p^3 \ ^3D^{\circ}$	(1%)	2	-334.2223244	417591.23	1.2025745[6]	-1.2597024[5]	2.247252[2]
$1s^2 2s 2p^3 \ ^1D^{\circ}$	(99%)			2	-333.7077365	530530.22	1.2007460[6]	-1.2674012[5]	2.241863[2]
$1s^2 2s 2p^3 \ ^3S^{\circ}$	(98%)	$+ 1s^2 2s 2p^3 \ ^1P^{\circ}$	(1%)	1	-333.6851524	535486.87	1.2006368[6]	-1.2584348[5]	2.238694[2]
$1s^2 2s 2p^3 \ ^1P^{\circ}$	(98%)	$+ 1s^2 2s 2p^3 \ ^3S^{\circ}$	(1%)	1	-333.4234398	592926.13	1.1997439[6]	-1.2438130[5]	2.241780[2]
$1s^2 2p^4 \ ^3P$	(97%)	$+ 1s^2 2s^2 2p^2 \ ^3P$	(1%)	2	-332.4255377	811940.33	1.1960775[6]	-1.6841870[5]	2.145211[2]
	(98%)	$+ 1s^2 2s^2 2p^2 \ ^3P$	(1%)	1	-332.3853807	820753.77	1.1959809[6]	-1.6856469[5]	2.145042[2]

Continued. . .

Table 10 (continued)

Level composition in LSJ coupling			J	Energy (E_h)	ΔE (cm^{-1})	\tilde{K}_{NMS} (GHz u)	\tilde{K}_{SMS} (GHz u)	\tilde{F} (GHz/fm ²)	
	(83%)	+ $1s^2 2s 2p^3 \ ^3D^o$	(13%)	1	-936.2380745	925023.66	3.3526794[6]	-4.1173409[5]	1.840368[3]
	(73%)	+ $1s^2 2s 2p^3 \ ^3D^o$	(17%)	2	-936.1581921	942555.81	3.3525300[6]	-4.1245870[5]	1.840274[3]
$1s^2 2s 2p^3 \ ^3S^o$	(79%)	+ $1s^2 2s 2p^3 \ ^1P^o$	(16%)	1	-935.4589964	1096011.52	3.3497898[6]	-4.1188479[5]	1.836400[3]
$1s^2 2s 2p^3 \ ^1D^o$	(92%)	+ $1s^2 2s 2p^3 \ ^3P^o$	(8%)	2	-935.3149284	1127630.80	3.3495320[6]	-4.1372183[5]	1.837670[3]
$1s^2 2s 2p^3 \ ^1P^o$	(81%)	+ $1s^2 2s 2p^3 \ ^3S^o$	(16%)	1	-934.7048425	1261529.17	3.3474528[6]	-4.1076184[5]	1.837118[3]
$1s^2 2p^4 \ ^3P$	(88%)	+ $1s^2 2p^4 \ ^1D$	(10%)	2	-932.9509614	1646461.57	3.3406037[6]	-5.4774917[5]	1.746354[3]
	(86%)	+ $1s^2 2p^4 \ ^1S$	(13%)	0	-932.5437626	1735831.37	3.3392999[6]	-5.4708499[5]	1.746275[3]
	(99%)	+ $1s^2 2s^2 2p^2 \ ^3P$	(1%)	1	-932.5220075	1740606.07	3.3393962[6]	-5.4944700[5]	1.745528[3]
$1s^2 2p^4 \ ^1D$	(89%)	+ $1s^2 2p^4 \ ^3P$	(10%)	2	-932.1703941	1817776.29	3.3381999[6]	-5.4977322[5]	1.745727[3]
$1s^2 2p^4 \ ^1S$	(83%)	+ $1s^2 2p^4 \ ^3P$	(13%)	0	-931.1191915	2048488.59	3.3345996[6]	-5.3766965[5]	1.749242[3]
Co XXII									
$1s^2 2s^2 2p^2 \ ^3P$	(88%)	+ $1s^2 2s^2 2p^2 \ ^1S$	(11%)	0	-1018.0790759	0.00	3.6429892[6]	-2.9717415[5]	2.291295[3]
	(99%)			1	-1017.6671163	90414.67	3.6419010[6]	-2.9832769[5]	2.291275[3]
	(72%)	+ $1s^2 2s^2 2p^2 \ ^1D$	(27%)	2	-1017.4487608	138338.16	3.6412960[6]	-2.9869958[5]	2.291123[3]
$1s^2 2s^2 2p^2 \ ^1D$	(71%)	+ $1s^2 2s^2 2p^2 \ ^3P$	(27%)	2	-1016.7946054	281908.67	3.6392466[6]	-3.0011628[5]	2.290388[3]
$1s^2 2s^2 2p^2 \ ^1S$	(86%)	+ $1s^2 2s^2 2p^2 \ ^3P$	(11%)	0	-1016.1846667	415774.75	3.6369910[6]	-3.0254646[5]	2.286263[3]
$1s^2 2s 2p^3 \ ^5S^o$	(95%)	+ $1s^2 2s 2p^3 \ ^3P^o$	(4%)	2	-1015.6451465	534185.74	3.6346037[6]	-4.5225833[5]	2.181290[3]
$1s^2 2s 2p^3 \ ^3D^o$	(82%)	+ $1s^2 2s 2p^3 \ ^3P^o$	(14%)	1	-1014.2805689	833675.90	3.6296349[6]	-4.5047741[5]	2.179718[3]
	(80%)	+ $1s^2 2s 2p^3 \ ^3P^o$	(18%)	2	-1014.2689159	836233.42	3.6296753[6]	-4.5084998[5]	2.179804[3]
	(100%)			3	-1014.1176006	869443.31	3.6294364[6]	-4.5225515[5]	2.179621[3]
$1s^2 2s 2p^3 \ ^3P^o$	(100%)			0	-1013.5788496	987685.47	3.6273378[6]	-4.4806718[5]	2.179621[3]
	(80%)	+ $1s^2 2s 2p^3 \ ^3D^o$	(15%)	1	-1013.5286534	998702.27	3.6272710[6]	-4.4896767[5]	2.179298[3]
	(68%)	+ $1s^2 2s 2p^3 \ ^3D^o$	(19%)	2	-1013.4295743	1020447.62	3.6270725[6]	-4.4981124[5]	2.179160[3]
$1s^2 2s 2p^3 \ ^3S^o$	(76%)	+ $1s^2 2s 2p^3 \ ^1P^o$	(18%)	1	-1012.7444302	1170819.36	3.6243484[6]	-4.4895136[5]	2.174925[3]
$1s^2 2s 2p^3 \ ^1D^o$	(89%)	+ $1s^2 2s 2p^3 \ ^3P^o$	(10%)	2	-1012.5539418	1212626.72	3.6239759[6]	-4.5102089[5]	2.176309[3]
$1s^2 2s 2p^3 \ ^1P^o$	(78%)	+ $1s^2 2s 2p^3 \ ^3S^o$	(18%)	1	-1011.8944485	1357368.78	3.6217341[6]	-4.4812204[5]	2.175562[3]
$1s^2 2p^4 \ ^3P$	(87%)	+ $1s^2 2p^4 \ ^1D$	(11%)	2	-1010.0936576	1752596.67	3.6146245[6]	-5.9701279[5]	2.067175[3]
	(83%)	+ $1s^2 2p^4 \ ^1S$	(16%)	0	-1009.6338604	1853510.51	3.6131211[6]	-5.9590652[5]	2.067195[3]
	(99%)	+ $1s^2 2s^2 2p^2 \ ^3P$	(1%)	1	-1009.5793390	1865476.56	3.6131623[6]	-5.9905233[5]	2.066077[3]
$1s^2 2p^4 \ ^1D$	(87%)	+ $1s^2 2p^4 \ ^3P$	(12%)	2	-1009.2171377	1944970.55	3.6119405[6]	-5.9938314[5]	2.066294[3]
$1s^2 2p^4 \ ^1S$	(80%)	+ $1s^2 2p^4 \ ^3P$	(16%)	0	-1008.0840049	2193664.45	3.6080964[6]	-5.8729051[5]	2.070166[3]
Ni XXIII									
$1s^2 2s^2 2p^2 \ ^3P$	(87%)	+ $1s^2 2s^2 2p^2 \ ^1S$	(12%)	0	-1098.8830366	0.00	3.9296269[6]	-3.2256649[5]	2.700763[3]
	(99%)			1	-1098.3830194	109741.08	3.9282849[6]	-3.2393718[5]	2.700723[3]
	(68%)	+ $1s^2 2s^2 2p^2 \ ^1D$	(31%)	2	-1098.1451334	161951.02	3.9276193[6]	-3.2429359[5]	2.700562[3]
$1s^2 2s^2 2p^2 \ ^1D$	(68%)	+ $1s^2 2s^2 2p^2 \ ^3P$	(31%)	2	-1097.4035318	324713.74	3.9253215[6]	-3.2617206[5]	2.699516[3]
$1s^2 2s^2 2p^2 \ ^1S$	(85%)	+ $1s^2 2s^2 2p^2 \ ^3P$	(12%)	0	-1096.7641427	465043.44	3.9229472[6]	-3.2860249[5]	2.694876[3]
$1s^2 2s 2p^3 \ ^5S^o$	(94%)	+ $1s^2 2s 2p^3 \ ^3P^o$	(5%)	2	-1096.2124762	586120.24	3.9204418[6]	-4.9086990[5]	2.569948[3]
$1s^2 2s 2p^3 \ ^3D^o$	(79%)	+ $1s^2 2s 2p^3 \ ^3P^o$	(16%)	1	-1094.8091024	894125.16	3.9153175[6]	-4.8889974[5]	2.568141[3]
	(78%)	+ $1s^2 2s 2p^3 \ ^3P^o$	(19%)	2	-1094.7835694	899729.01	3.9153398[6]	-4.8946498[5]	2.568257[3]
	(100%)			3	-1094.5956060	940982.21	3.9150099[6]	-4.9105593[5]	2.568012[3]
$1s^2 2s 2p^3 \ ^3P^o$	(100%)			0	-1094.0319421	1064692.14	3.9127977[6]	-4.8665168[5]	2.568010[3]
	(77%)	+ $1s^2 2s 2p^3 \ ^3D^o$	(17%)	1	-1093.9691946	1078463.62	3.9127002[6]	-4.8772063[5]	2.567564[3]
	(64%)	+ $1s^2 2s 2p^3 \ ^3D^o$	(21%)	2	-1093.8489125	1104862.49	3.9124450[6]	-4.8868652[5]	2.567363[3]
$1s^2 2s 2p^3 \ ^3S^o$	(73%)	+ $1s^2 2s 2p^3 \ ^1P^o$	(20%)	1	-1093.1839384	1250807.44	3.9097607[6]	-4.8751369[5]	2.562787[3]
$1s^2 2s 2p^3 \ ^1D^o$	(87%)	+ $1s^2 2s 2p^3 \ ^3P^o$	(12%)	2	-1092.9371159	1304978.71	3.9092456[6]	-4.8984596[5]	2.564290[3]
$1s^2 2s 2p^3 \ ^1P^o$	(76%)	+ $1s^2 2s 2p^3 \ ^3S^o$	(20%)	1	-1092.2247859	1461317.07	3.9068272[6]	-4.8702270[5]	2.563294[3]
$1s^2 2p^4 \ ^3P$	(86%)	+ $1s^2 2p^4 \ ^1D$	(13%)	2	-1090.3869559	1864674.11	3.8994837[6]	-6.4826409[5]	2.434579[3]
	(80%)	+ $1s^2 2p^4 \ ^1S$	(19%)	0	-1089.8737589	1977307.82	3.8977729[6]	-6.4662982[5]	2.434751[3]
	(99%)	+ $1s^2 2s^2 2p^2 \ ^3P$	(1%)	1	-1089.7747529	1999037.13	3.8977270[6]	-6.5069208[5]	2.433135[3]
$1s^2 2p^4 \ ^1D$	(86%)	+ $1s^2 2p^4 \ ^3P$	(13%)	2	-1089.4021877	2080805.75	3.8964817[6]	-6.5103155[5]	2.433372[3]
$1s^2 2p^4 \ ^1S$	(77%)	+ $1s^2 2p^4 \ ^3P$	(20%)	0	-1088.1753696	2350061.20	3.8923608[6]	-6.3908806[5]	2.437562[3]

Table 11

Comparison of corrected (K_{SMS}) and uncorrected (K_{SMS}^1) specific shift parameters (in $m_e E_h$) for several states of N II, O III, F IV, Ne V and Ti XVII. See page 17 for explanations.

Level	J	N II			O III			F IV		
		[53]	This work		[53]	This work		[53]	This work	
		K_{SMS}^1	K_{SMS}^1	K_{SMS}	K_{SMS}^1	K_{SMS}^1	K_{SMS}	K_{SMS}^1	K_{SMS}^1	K_{SMS}
$2s^2 2p^2 \ ^3P$	0	-1.280	-1.278	-1.275	-2.473	-2.471	-2.461	-3.984	-3.983	-3.963
	1	-1.279	-1.277	-1.275	-2.471	-2.469	-2.462	-3.981	-3.980	-3.964
	2	-1.278	-1.276	-1.276	-2.468	-2.467	-2.464	-3.977	-3.976	-3.967
$2s^2 2p^2 \ ^1D$	2	-1.236	-1.239	-1.237	-2.422	-2.423	-2.418	-3.926	-3.927	-3.915
$2s^2 2p^2 \ ^1S$	0	-1.230	-1.237	-1.236	-2.415	-2.420	-2.414	-3.924	-3.927	-3.915
$2s 2p^3 \ ^5S^o$	2	-2.487	-2.481	-2.477	-4.323	-4.316	-4.306	-6.631	-6.624	-6.602
$2s 2p^3 \ ^3D^o$	3	-2.387	-2.386	-2.382	-4.208	-4.208	-4.198	-6.506	-6.505	-6.484
	2	-2.387	-2.386	-2.382	-4.208	-4.208	-4.197	-6.505	-6.505	-6.483
	1	-2.387	-2.387	-2.383	-4.208	-4.208	-4.198	-6.504	-6.505	-6.483
$2s 2p^3 \ ^3P^o$	2	-2.250	-2.251	-2.247	-4.025	-4.028	-4.018	-6.277	-6.279	-6.258
	1	-2.250	-2.251	-2.248	-4.025	-4.027	-4.017	-6.277	-6.279	-6.257
	0	-2.250	-2.251	-2.248	-4.026	-4.028	-4.017	-6.277	-6.279	-6.257
$2s 2p^3 \ ^1D^o$	2	-2.127	-2.133	-2.129	-3.918	-3.920	-3.909	-6.199	-6.200	-6.177
$2s 2p^3 \ ^3S^o$	1	—	-1.768	-1.764	-3.592	-3.590	-3.579	-5.895	-5.893	-5.868
$2s 2p^3 \ ^1P^o$	1	—	-1.461	-1.457	-3.569	-3.583	-3.572	-5.830	-5.841	-5.819
Level	J	Ne V			Ti XVII					
		[53]	This work		[53]	This work				
		K_{SMS}^1	K_{SMS}^1	K_{SMS}	K_{SMS}^1	K_{SMS}^1	K_{SMS}			
$2s^2 2p^2 \ ^3P$	0	-5.816	-5.815	-5.776	-53.279	-53.279	-51.182			
	1	-5.810	-5.809	-5.779	-52.831	-52.831	-51.305			
	2	-5.802	-5.801	-5.784	-52.647	-52.647	-51.402			
$2s^2 2p^2 \ ^1D$	2	-5.748	-5.750	-5.726	-52.393	-52.395	-51.396			
$2s^2 2p^2 \ ^1S$	0	-5.758	-5.760	-5.736	-52.897	-52.908	-51.935			
$2s 2p^3 \ ^5S^o$	2	-9.411	-9.404	-9.364	-80.082	-80.066	-78.032			
$2s 2p^3 \ ^3D^o$	3	-9.277	-9.277	-9.237	-79.832	-79.829	-77.904			
	2	-9.276	-9.276	-9.236	-79.937	-79.933	-77.754			
	1	-9.276	-9.276	-9.236	-79.936	-79.933	-77.751			
$2s 2p^3 \ ^3P^o$	2	-9.002	-9.004	-8.965	-78.863	-78.863	-77.193			
	1	-9.001	-9.004	-8.964	-78.937	-78.937	-77.103			
	0	-9.001	-9.003	-8.964	-78.946	-78.946	-77.027			
$2s 2p^3 \ ^1D^o$	2	-8.961	-8.963	-8.921	-79.407	-79.407	-77.564			
$2s 2p^3 \ ^3S^o$	1	-8.674	-8.672	-8.628	-79.405	-79.402	-77.238			
$2s 2p^3 \ ^1P^o$	1	-8.556	-8.566	-8.525	-78.355	-78.360	-76.737			

Table 12

Comparison of MCHF and MCDHF specific mass shift parameters for O III (in atomic units $E_h m_e$).

	MCHF K_{SMS}^1	MCDHF		
		J	K_{SMS}^1	K_{SMS}
$1s^2 2s^2 2p^2 \ ^3P$	-2.4877	0	-2.4710	-2.4614
		1	-2.4695	-2.4621
		2	-2.4671	-2.4638
$1s^2 2s^2 2p^2 \ ^1D$	-2.4316	2	-2.4232	-2.4181
$1s^2 2s^2 2p^2 \ ^1S$	-2.4171	0	-2.4195	-2.4144
$1s^2 2s 2p^3 \ ^5S^o$	-4.3259	2	-4.3164	-4.3061
$1s^2 2s 2p^3 \ ^3D^o$	-4.2151	3	-4.2078	-4.1978
		2	-4.2077	-4.1974
		1	-4.2082	-4.1978
$1s^2 2s 2p^3 \ ^3P^o$	-4.0183	2	-4.0280	-4.0182
		1	-4.0275	-4.0174
		0	-4.0276	-4.0175
$1s^2 2s 2p^3 \ ^1D^o$	-3.9245	2	-3.9200	-3.9094
$1s^2 2s 2p^3 \ ^3S^o$	-3.5915	1	-3.5903	-3.5786
$1s^2 2s 2p^3 \ ^1P^o$	-3.5399	1	-3.5825	-3.5720
$1s^2 2p^4 \ ^3P$	-5.5479	2	-5.5704	-5.5532
		1	-5.5680	-5.5545
		0	-5.5666	-5.5549
$1s^2 2p^4 \ ^1D$	-5.7031	2	-5.7273	-5.7124

Table 13

Total energies (in E_h), excitation energies (in cm^{-1}), normal and specific mass shift \tilde{K} parameters (in GHz u), \tilde{F} field shift factors (in GHz/fm^2) for levels in the nitrogen isoelectronic sequence ($7 \leq Z \leq 36$ and $Z = 42, 74$). For each of the many-electron wave functions, the leading components are given in the LSJ coupling scheme. The number in square brackets is the power of 10. See page 18 for Explanation of Tables.

Level composition in LSJ coupling		J	Energy (E_h)	ΔE (cm^{-1})	\tilde{K}_{NMS} (GHz u)	\tilde{K}_{SMS} (GHz u)	\tilde{F} (GHz/fm^2)
N I							
$2s^2 2p^3 \ ^4S^o$ (96%)	+ $2s 2p^3 3d \ ^4S^o$ (2%)	3/2	-54.6073794	0.00	1.9688775[5]	-6.3040379[3]	7.239658
$2s^2 2p^3 \ ^2D^o$ (96%)	+ $2s 2p^3 3d \ ^2D^o$ (1%)	5/2	-54.5185543	19494.84	1.9662690[5]	-6.1196713[3]	7.245065
(96%)	+ $2s 2p^3 3d \ ^2D^o$ (1%)	3/2	-54.5185222	19501.91	1.9662598[5]	-6.1185845[3]	7.245077
$2s^2 2p^3 \ ^2P^o$ (93%)	+ $2p^5 \ ^2P^o$ (3%)	3/2	-54.4735477	29372.66	1.9648715[5]	-6.1771300[3]	7.241464
(93%)	+ $2p^5 \ ^2P^o$ (3%)	1/2	-54.4735265	29377.32	1.9648663[5]	-6.1780280[3]	7.241484
$2s 2p^4 \ ^4P$ (91%)	+ $2s^2 2p^2 3d \ ^4P$ (3%)	5/2	-54.2058086	88134.61	1.9543893[5]	-9.7150959[3]	7.090616
(91%)	+ $2s^2 2p^2 3d \ ^4P$ (3%)	3/2	-54.2055167	88198.66	1.9543814[5]	-9.7145389[3]	7.090708
(91%)	+ $2s^2 2p^2 3d \ ^4P$ (3%)	1/2	-54.2053304	88239.55	1.9543757[5]	-9.7192933[3]	7.090752
O II							
$2s^2 2p^3 \ ^4S^o$ (97%)	+ $2s 2p^3 3d \ ^4S^o$ (1%)	3/2	-74.6062512	0.00	2.6897257[5]	-1.2214679[4]	1.265142[1]
$2s^2 2p^3 \ ^2D^o$ (97%)	+ $2s 2p^3 3d \ ^2D^o$ (1%)	5/2	-74.4831059	27027.27	2.6857762[5]	-1.1981788[4]	1.265835[1]
(97%)	+ $2s 2p^3 3d \ ^2D^o$ (1%)	3/2	-74.4830197	27046.19	2.6857602[5]	-1.1979832[4]	1.265837[1]
$2s^2 2p^3 \ ^2P^o$ (95%)	+ $2p^5 \ ^2P^o$ (3%)	3/2	-74.4202118	40830.92	2.6836849[5]	-1.2024687[4]	1.264950[1]
(95%)	+ $2p^5 \ ^2P^o$ (3%)	1/2	-74.4201846	40836.89	2.6836754[5]	-1.2024924[4]	1.264953[1]
$2s 2p^4 \ ^4P$ (96%)	+ $2s^2 2p^2 3d \ ^4P$ (2%)	5/2	-74.0588300	120145.06	2.6701545[5]	-1.7573247[4]	1.233499[1]
(96%)	+ $2s^2 2p^2 3d \ ^4P$ (2%)	3/2	-74.0580811	120309.43	2.6701398[5]	-1.7575393[4]	1.233504[1]
(96%)	+ $2s^2 2p^2 3d \ ^4P$ (2%)	1/2	-74.0576760	120398.33	2.6701412[5]	-1.7580201[4]	1.233507[1]
$2s 2p^4 \ ^2D$ (93%)	+ $2s^2 2p^2 3d \ ^2D$ (3%)	5/2	-73.8469156	166654.88	2.6632125[5]	-1.7063524[4]	1.233145[1]
(93%)	+ $2s^2 2p^2 3d \ ^2D$ (3%)	3/2	-73.8468823	166662.20	2.6631989[5]	-1.7061358[4]	1.233147[1]
$2s 2p^4 \ ^2S$ (93%)	+ $2s^2 2p^2 3d \ ^2S$ (2%)	1/2	-73.7069689	197369.64	2.6587044[5]	-1.6141558[4]	1.233614[1]
F III							
$2s^2 2p^3 \ ^4S^o$ (98%)	+ $2s 2p^3 3d \ ^4S^o$ (1%)	3/2	-97.8791584	0.00	3.5283141[5]	-1.9807514[4]	2.070857[1]
$2s^2 2p^3 \ ^2D^o$ (98%)		5/2	-97.7228884	34297.31	3.5231120[5]	-1.9539214[4]	2.071721[1]
(98%)		3/2	-97.7227397	34329.92	3.5230855[5]	-1.9535973[4]	2.071723[1]
$2s^2 2p^3 \ ^2P^o$ (96%)	+ $2p^5 \ ^2P^o$ (3%)	3/2	-97.6427889	51877.10	3.5203727[5]	-1.9577071[4]	2.069970[1]
(96%)	+ $2p^5 \ ^2P^o$ (3%)	1/2	-97.6427648	51882.40	3.5203589[5]	-1.9576162[4]	2.069977[1]
$2s 2p^4 \ ^4P$ (97%)	+ $2s^2 2p^2 3d \ ^4P$ (1%)	5/2	-97.1862603	152073.55	3.5035841[5]	-2.7669163[4]	2.012156[1]
(97%)	+ $2s^2 2p^2 3d \ ^4P$ (1%)	3/2	-97.1847236	152410.82	3.5035556[5]	-2.7673491[4]	2.012163[1]
(97%)	+ $2s^2 2p^2 3d \ ^4P$ (1%)	1/2	-97.1839059	152590.29	3.5035533[5]	-2.7679566[4]	2.012168[1]
$2s 2p^4 \ ^2D$ (96%)	+ $2s^2 2p^2 3d \ ^2D$ (2%)	5/2	-96.9191468	210698.18	3.4945896[5]	-2.7095134[4]	2.010674[1]
(96%)	+ $2s^2 2p^2 3d \ ^2D$ (2%)	3/2	-96.9190754	210713.85	3.4945744[5]	-2.7091709[4]	2.010676[1]
$2s 2p^4 \ ^2S$ (96%)	+ $2s^2 2p^2 3d \ ^2S$ (1%)	1/2	-96.7437767	249187.47	3.4887923[5]	-2.5930544[4]	2.010852[1]
$2s 2p^4 \ ^2P$ (95%)	+ $2s^2 2p^2 3d \ ^2P$ (2%)	3/2	-96.6603346	267500.89	3.4857952[5]	-2.5220115[4]	2.005521[1]
(95%)	+ $2s^2 2p^2 3d \ ^2P$ (2%)	1/2	-96.6585348	267895.90	3.4857751[5]	-2.5228975[4]	2.005528[1]
Ne IV							
$2s^2 2p^3 \ ^4S^o$ (98%)	+ $2s 2p^3 3d \ ^4S^o$ (1%)	3/2	-124.4241779	0.00	4.4844166[5]	-2.9081654[4]	3.219648[1]
$2s^2 2p^3 \ ^2D^o$ (98%)		5/2	-124.2353345	41446.34	4.4780094[5]	-2.8784180[4]	3.220703[1]
(98%)		3/2	-124.2351338	41490.39	4.4779676[5]	-2.8778953[4]	3.220704[1]
$2s^2 2p^3 \ ^2P^o$ (96%)	+ $2p^5 \ ^2P^o$ (3%)	1/2	-124.1383198	62738.60	4.4746248[5]	-2.8826992[4]	3.217634[1]
(96%)	+ $2p^5 \ ^2P^o$ (3%)	3/2	-124.1383032	62742.26	4.4746443[5]	-2.8830038[4]	3.217620[1]
$2s 2p^4 \ ^4P$ (98%)	+ $2s^2 2p^2 3d \ ^4P$ (1%)	5/2	-123.5858394	183994.04	4.4544547[5]	-4.0014177[4]	3.119539[1]
(98%)	+ $2s^2 2p^2 3d \ ^4P$ (1%)	3/2	-123.5830378	184608.91	4.4543991[5]	-4.0021519[4]	3.119547[1]
(98%)	+ $2s^2 2p^2 3d \ ^4P$ (1%)	1/2	-123.5815480	184935.88	4.4543872[5]	-4.0029521[4]	3.119554[1]
$2s 2p^4 \ ^2D$ (97%)	+ $2s^2 2p^2 3d \ ^2D$ (1%)	5/2	-123.2646630	254484.10	4.4434692[5]	-3.9387805[4]	3.116674[1]
(97%)	+ $2s^2 2p^2 3d \ ^2D$ (1%)	3/2	-123.2645505	254508.79	4.4434501[5]	-3.9382557[4]	3.116677[1]
$2s 2p^4 \ ^2S$ (97%)	+ $2s^2 2p^2 3d \ ^2S$ (1%)	1/2	-123.0555597	300376.97	4.4364040[5]	-3.7966734[4]	3.116802[1]
$2s 2p^4 \ ^2P$ (97%)	+ $2s^2 2p^2 3d \ ^2P$ (1%)	3/2	-122.9632230	320642.53	4.4329602[5]	-3.7452495[4]	3.107733[1]
(97%)	+ $2s^2 2p^2 3d \ ^2P$ (1%)	1/2	-122.9599401	321363.04	4.4329122[5]	-3.7466402[4]	3.107741[1]
$2p^5 \ ^2P^o$ (92%)	+ $2s^2 2p^3 \ ^2P^o$ (2%)	3/2	-122.2118055	485559.61	4.4064374[5]	-4.8671521[4]	3.015478[1]
(92%)	+ $2s^2 2p^3 \ ^2P^o$ (2%)	1/2	-122.2073660	486533.97	4.4063930[5]	-4.8695798[4]	3.015456[1]
Na V							
$2s^2 2p^3 \ ^4S^o$ (99%)	+ $2s 2p^3 3d \ ^4S^o$ (1%)	3/2	-154.2425695	0.00	5.5579352[5]	-4.0030759[4]	4.801120[1]
$2s^2 2p^3 \ ^2D^o$ (99%)		5/2	-154.0214506	48529.98	5.5503516[5]	-3.9707876[4]	4.802385[1]
(98%)		3/2	-154.0212512	48573.76	5.5502899[5]	-3.9699611[4]	4.802379[1]
$2s^2 2p^3 \ ^2P^o$ (97%)	+ $2p^5 \ ^2P^o$ (2%)	1/2	-153.9076866	73498.31	5.5463433[5]	-3.9769671[4]	4.797393[1]
(96%)	+ $2p^5 \ ^2P^o$ (2%)	3/2	-153.9075339	73531.81	5.5463704[5]	-3.9776511[4]	4.797366[1]
$2s 2p^4 \ ^4P$ (99%)		5/2	-153.2585529	215966.69	5.5227174[5]	-5.4598027[4]	4.640873[1]
(99%)		3/2	-153.2538432	217000.33	5.5226178[5]	-5.4609559[4]	4.640878[1]
(99%)		1/2	-153.2513363	217550.55	5.5225882[5]	-5.4620193[4]	4.640886[1]
$2s 2p^4 \ ^2D$ (98%)	+ $2s^2 2p^2 3d \ ^2D$ (1%)	5/2	-152.8836571	298246.80	5.5097872[5]	-5.3932251[4]	4.636207[1]
(98%)	+ $2s^2 2p^2 3d \ ^2D$ (1%)	3/2	-152.8835013	298281.00	5.5097623[5]	-5.3924393[4]	4.636211[1]

Continued. . .

Table 13 (continued)

Level composition in LSJ coupling				J	Energy (E_h)	ΔE (cm^{-1})	\tilde{K}_{NMS} (GHz u)	\tilde{K}_{SMS} (GHz u)	\tilde{F} (GHz/fm 2)
$2s^2 2p^3 \ ^2P^o$	(41%)	+ $2s^2 2p^3 \ ^4S^o$	(36%)	3/2	-2749.7273173	0.00	9.7261275[6]	-1.1458348[6]	1.855781[4]
$2s^2 2p^3 \ ^4S^o$	(50%)	+ $2s^2 2p^3 \ ^2D^o$	(48%)	3/2	-2746.0988862	796348.57	9.7150883[6]	-1.1556487[6]	1.855011[4]
$2s^2 2p^3 \ ^2D^o$	(100%)			5/2	-2745.5180675	923823.52	9.7135763[6]	-1.1559409[6]	1.855036[4]
$2s^2 2p^3 \ ^2P^o$	(99%)			1/2	-2744.7460262	1093266.99	9.7102563[6]	-1.1552912[6]	1.853940[4]
	(55%)	+ $2s^2 2p^3 \ ^2D^o$	(29%)	3/2	-2741.1042042	1892554.51	9.6994982[6]	-1.1696174[6]	1.852247[4]
$2s2p^4 \ ^4P$	(83%)	+ $2s2p^4 \ ^2D$	(17%)	5/2	-2740.4215834	2042372.47	9.6940252[6]	-1.5401785[6]	1.757102[4]
	(49%)	+ $2s2p^4 \ ^2S$	(47%)	1/2	-2738.7235517	2415047.34	9.6877959[6]	-1.5348400[6]	1.756630[4]
$2s2p^4 \ ^2D$	(83%)	+ $2s2p^4 \ ^4P$	(17%)	5/2	-2735.2190483	3184196.90	9.6777034[6]	-1.5483715[6]	1.755315[4]
$2s2p^4 \ ^2P$	(53%)	+ $2s2p^4 \ ^4P$	(32%)	1/2	-2734.3534636	3374170.78	9.6742524[6]	-1.5440566[6]	1.754397[4]
	(44%)	+ $2s2p^4 \ ^2S$	(38%)	1/2	-2730.0641923	4315556.98	9.6610009[6]	-1.5515314[6]	1.753265[4]
$2p^5 \ ^2P^o$	(99%)	+ $2s^2 2p^3 \ ^2P^o$	(1%)	3/2	-2727.6045428	4855387.65	9.6490752[6]	-1.9131285[6]	1.658336[4]
	(99%)	+ $2s^2 2p^3 \ ^2P^o$	(1%)	1/2	-2723.4503387	5767130.03	9.6364344[6]	-1.9265111[6]	1.656062[4]
W LXVIII									
$2s^2 2p^3 \ ^2P^o$	(49%)	+ $2s^2 2p^3 \ ^2D^o$	(27%)	3/2	-9302.7182563	0.00	3.1051381[7]	-3.2315779[6]	5.054766[5]
$2s^2 2p^3 \ ^4S^o$	(55%)	+ $2s^2 2p^3 \ ^2D^o$	(45%)	3/2	-9251.0505799	11339743.90	3.0886313[7]	-3.4384315[6]	5.037473[5]
$2s^2 2p^3 \ ^2D^o$	(100%)			5/2	-9249.8310483	11607400.14	3.0882627[7]	-3.4385258[6]	5.037493[5]
$2s^2 2p^3 \ ^2P^o$	(100%)			1/2	-9248.3654393	11929064.12	3.0877449[7]	-3.4313786[6]	5.037197[5]
$2s2p^4 \ ^2S$	(65%)	+ $2s2p^4 \ ^4P$	(25%)	1/2	-9235.2148740	14815279.51	3.0860275[7]	-4.4304563[6]	4.726262[5]
$2s2p^4 \ ^2P$	(52%)	+ $2s2p^4 \ ^2D$	(35%)	3/2	-9234.9227026	14879403.72	3.0859816[7]	-4.4165435[6]	4.724963[5]
$2s^2 2p^3 \ ^2P^o$	(51%)	+ $2s^2 2p^3 \ ^2D^o$	(28%)	3/2	-9196.4732118	23318091.30	3.0712310[7]	-3.6530543[6]	5.016029[5]
$2s2p^4 \ ^4P$	(85%)	+ $2s2p^4 \ ^2D$	(10%)	3/2	-9186.2604959	25559523.29	3.0703680[7]	-4.6432241[6]	4.709432[5]
$2s2p^4 \ ^2P$	(65%)	+ $2s2p^4 \ ^4P$	(35%)	1/2	-9182.3586975	26415869.03	3.0691766[7]	-4.6116068[6]	4.706982[5]
$2s2p^4 \ ^2D$	(55%)	+ $2s2p^4 \ ^2P$	(44%)	3/2	-9181.8460915	26528373.04	3.0690350[7]	-4.6112499[6]	4.707171[5]
$2p^5 \ ^2P^o$	(99%)			3/2	-9168.5689588	29442366.76	3.0670564[7]	-5.6011064[6]	4.399653[5]
$2s2p^4 \ ^4P$	(40%)	+ $2s2p^4 \ ^2S$	(35%)	1/2	-9130.0438073	37897659.95	3.0524448[7]	-4.8190543[6]	4.690210[5]
$2p^5 \ ^2P^o$	(100%)			1/2	-9115.7785445	41028523.14	3.0502636[7]	-5.7962112[6]	4.377606[5]

Table 14

Comparison of MCHF and MCDHF specific mass shift parameters for Ne IV (in atomic units $E_h m_e$).

	MCHF	MCDHF		
	K_{SMS}^1	J	K_{SMS}^1	K_{SMS}
$2s^2 2p^3 \ ^4S^o$	-8.1008	3/2	-8.0918	-8.0570
$2s^2 2p^3 \ ^2D^o$	-8.0133	5/2	-8.0086	-7.9746
		3/2	-8.0083	-7.9732
$2s^2 2p^3 \ ^2P^o$	-8.0209	1/2	-8.0207	-7.9865
		3/2	-8.0204	-7.9873
$2s2p^4 \ ^4P$	-11.1298	5/2	-11.1401	-11.0858
		3/2	-11.1326	-11.0879
		1/2	-11.1292	-11.0901
$2s2p^4 \ ^2D$	-10.9247	5/2	-10.9608	-10.9123
		3/2	-10.9599	-10.9109
$2s2p^4 \ ^2S$	-10.5174	1/2	-10.5672	-10.5186
$2s2p^4 \ ^2P$	-10.4440	3/2	-10.4310	-10.3761
		1/2	-10.4228	-10.3800
$2p^5 \ ^2P^o$	-13.4948	3/2	-13.5525	-13.4843
		1/2	-13.5426	-13.4911